Available online at www.sciencedirect.com

SciVerse ScienceDirect

Geochimica et Cosmochimica Acta 104 (2013) 261–280

Geochimica et Cosmochimica Acta

www.elsevier.com/locate/gca

A new approach for measuring dissolution rates of silicate minerals by using silicon isotopes

Chen Gruber [a,*,1], Liat Harpaz [a,1], Chen Zhu [b], Tom D. Bullen [c], Jiwchar Ganor [a]

[a] Department of Geological and Environmental Sciences, Ben-Gurion University of the Negev, P.O. Box 653, Beer-Sheva 84105, Israel
[b] Department of Geological Sciences, Indiana University, Bloomington, IN 47405, USA
[c] U.S. Geological Survey, Menlo Park, CA 94025, USA

Received 24 June 2012; accepted in revised form 14 November 2012; Available online 29 November 2012

Abstract

The two major problems in measuring dissolution rates under close-to-natural conditions in laboratory experiments are: (1) our inability to measure small differences in concentration between solutions with relatively high concentrations and (2) the inherent problem that the change in solution concentration is affected by both the dissolution of the primary mineral and the precipitation of secondary minerals. The present manuscript proposes and tests a novel method, "the isotope ratio method", for measuring slow dissolution rates of silicate minerals by measuring the change in the ratios between stable isotopes of silicon of a spiked solution.

Based on mass balance calculations, two equations that describe the dissolution rate of a silicate mineral in a batch reactor and in a flow-through reactor at steady-state are developed. The precipitation rate of the secondary mineral may be calculated by subtracting the release rate of Si that was calculated using isotope dilution from the rate that was calculated using the proposed isotope ratio method.

Numerical simulations of flow-through and batch experiments demonstrate that the "isotope ratio method" is significantly more precise than conventional methods. The analytical uncertainty for the determination of dissolution rates was found to be low for the entire range of reported field-based dissolution rates. The calculation showed that even relatively large isotopic fractionations (up to ε values of 20‰), introduce insignificant uncertainties.

Preliminary flow-through experiments support the above conclusion that dissolution rate may be obtained accurately and with small uncertainty using the proposed "isotope ratio method".

1. INTRODUCTION

One of the most basic problems in studying weathering kinetics is the discrepancy between dissolution rates of silicate minerals measured in the field and dissolution rates measured in laboratory experiments. The rates measured in the laboratory are faster by a few orders of magnitude than the rates in the field (Schnoor, 1990; Stumm, 1992; van Grinsven and van Riemsdijk, 1992; Anbeek, 1993; Casey et al., 1993; Velbel, 1993; Blum and Stillings, 1995; White and Brantley, 1995, 2003; Drever, 2003; Zhu et al., 2004; Zhu, 2005; Ganor et al., 2007). The many differences between experimental conditions in the laboratory and natural conditions in the field were thoroughly discussed in previous studies (e.g., White and Brantley, 2003, and references therein). In short, these differences result from: efficiency of solution/mineral contact, duration of weathering, aging of surfaces, presence and depth of defects and etch pits, formation of leached layers, surface coatings, degree of undersaturation, and solution chemistry in micro-pores.

In contrast to natural weathering, laboratory experiments are usually conducted under conditions in which pre-

* Corresponding author. Tel.: +972 8 6477 517; fax: +972 8 6472 997.
E-mail address: chengrub@post.bgu.ac.il (C. Gruber).
[1] These authors contributed equally to this work.

0016-7037/$ - see front matter © 2012 Elsevier Ltd. All rights reserved.
http://dx.doi.org/10.1016/j.gca.2012.11.022

cipitation of secondary phases does not occur. Precipitation of secondary phases has mainly two effects on dissolution rates of primary minerals (Ganor et al., 2007; Maher et al., 2009; Steefel and Maher, 2009; Zhu et al., 2010): (1) Coating the surface area of the primary mineral, reducing the contact area of the solution with the mineral. (2) Preventing the solution from reaching equilibrium. The first effect slows the dissolution reaction while the second effect accelerates dissolution.

The many different experimental designs (e.g., pH-stat, stirred batch, fluidized bed, stirred flow-through and column) that are available to determine dissolution rates may be classified into three generic groups: batch, mixed flow-through and column experiments. In all these methods, determination of dissolution rates of silicates is usually based on differences between measurements of Si concentrations. However, the change in solution concentration is affected by both the dissolution of the primary mineral and the precipitation of secondary minerals. Moreover, these concentration differences are small relative to the high concentration of the experimental solutions, under relatively close-to-equilibrium conditions. To overcome these problems, most laboratory experiments are conducted under far-from-equilibrium conditions and are designed to avoid precipitation of secondary phases (Casey et al., 1993). In contrast, weathering in the field occurs relatively close-to equilibrium (White and Brantley, 2003) and tends to be incongruent due to the precipitation of secondary minerals. Moreover, the slow dissolution rates of the primary minerals under natural weathering conditions create only minute changes in concentration of the ions which are released to the solution such as silicon and aluminum. As the change in concentration is lower than the uncertainty on ion concentration measurement, the uncertainty on the measured rate is large. As a result, the slow rates of mineral dissolution that are observed in the field cannot be determined using standard laboratory methods (Ganor et al., 2007). Therefore, a new method for measuring incongruent and slow dissolution reactions is needed.

This paper proposes and tests a novel method for measuring slow dissolution rates of silicate minerals by using stable isotopes of Silicon. This new method overcomes the analytical difficulties by lowering the absolute uncertainty on dissolution rates. Moreover, with this method one can eliminate the effect of secondary phase precipitation on the determination of dissolution rate of a primary mineral and it is possible to approximate the precipitation rate of the secondary phase minerals.

2. EXPERIMENTAL METHODS

2.1. Numerical simulations

For a geochemical system that has n species, the following ordinary differential equations define the geochemical reaction network in a well-mixed reactor (Helgeson et al., 1970; Zhu et al., 2010):

$$\frac{dC_i}{dt} = \sum_j \upsilon_{i,j} r_{i,j}, i \in n \quad (1)$$

where C_i denotes concentrations of ith species, t is time, υ is the stoichiometric coefficient for ith species in the jth reaction and $r_{i,j}$ is the consumption or production rate of ith species in the jth reaction. In the present study, this set of equations was solved using the computer code P_{HREEQC} (Parkhurst and Appello, 1999), with Zhu et al. (2010) database for equilibrium constants at appropriate temperatures and pressures and reactions rate laws as described in Section 3.2 below. The extended Debye–Hückel equation was used for calculating activity coefficients of charged aqueous species, and the Setchénow equation with a coefficient of 0.1 was used for calculating activity coefficients of uncharged aqueous species. In all calculations we assumed that all homogenous reactions were instantaneous and therefore all aqueous species were in equilibrium with each other. Solutions were charged balanced with chlorine ions. The chlorine ions concentration changed by less than 10^{-5}% during and in the end of the simulation compared to the beginning.

2.2. Albite sample

The sample used in this study is the Amelia Court House albite from Ward's Scientific Est. The composition of the sample ($Ab_{99.8}$) was determined using EDS electron microprobe by Beig & Lüttge (2006). Based on a single measurement, the isotopic composition of the silicon in the Amelia Court House albite is $\delta^{29}Si$ (NBS-28) $= -0.110‰$ and $\delta^{30}Si$ (NBS-28) $= -0.256‰$ ($^{29}Si/^{28}Si = 0.05063$ and $^{30}Si/^{28}Si = 0.03361$) (Karen Ziegler, personal communication). Within uncertainty of the absolute value of NBS-28 (Barnes et al., 1975), these isotope ratios are the same as that of NBS-28 (0.0506327 ± 0.0000315 and 0.03362113 ± 0.0000084, respectively).

The albite was ground with an agate pestle and mortar and then sieved to a particle size of 25–53 μm. The specific surface area was measured by multipoint Brunauer–Emmett–Teller (BET) method (Brunauer et al., 1938), and is equal 0.39 ± 0.04 m^2 g^{-1}. The initial weight of the albite sample used in this experiment was 0.5002 ± 0.0001 g. Less than 1% of the mass of the albite was dissolved during the experiment.

2.3. Experimental setting

The experiment was carried out using a flow-through reactor fully immersed in a thermostatic water bath held at a constant temperature. The first 2700 h of the experiment were held at a constant temperature of 50 °C. This allowed the experiment to reach a steady state much faster, due to the rapid dissolution of the more reactive surfaces of the albite crystals. After that period of time the reactor was transferred to a bath with a constant temperature of 25 °C.

The reaction cell is a closed cylinder of Lexan plastic that is composed of two chambers, a lower chamber of 33-mm inner diameter and an upper chamber of 26-mm inner diameter. The two chambers are separated by a fine (5 μm) nylon mesh, on which mineral powders are placed. The flow rate, which was controlled by a peristaltic pump, was $7.60 \pm 0.09 \times 10^{-8}$ L s^{-1}. Solutions were filtered on the

outflow side with a 0.45 μm Durapore membrane (Millipore).

2.4. Inflow solutions

Isotopically enriched inflow solutions (henceforth "experimental spike") were prepared by mixing two solutions with different $^{29}Si/^{28}Si$ isotopic ratio. The first solution used was a silicon standard solution with a natural isotopic ratio. The second solution was a spiked solution that was prepared by dissolving SiO_2 powder enriched with ^{29}Si isotope (from Isoflex USA) with analytical quality KOH 45%. The pH of the inflow solution was then reduced using 1.2 M HCl to be in the range of 4.8–5.2. The nominal abundance of ^{29}Si in the SiO_2 powder was 96.74%. The abundance of ^{29}Si in the inflow solution was $8.53 \pm 0.04\%$ (almost twice the natural abundance of ^{29}Si, which is 4.671%). The Si concentration of the inflow solutions were 197 ± 8 μM (see Table 1 for the measured Si concentration and isotopic composition of each of the samples). Two batches of inflow solution were made during the experiment. The switch between the two solutions occurred at time 5400 h.

2.5. Analytical methods

Total Si and Al concentrations of the spike solution and the inflow and outflow solutions were analyzed using Inductively Coupled Plasma-Quadruple Mass Spectrometry (ICP-QMS). Silicon and aluminum concentrations were determined relative to calibration curves developed with synthetic multi-element standards, prepared from single element concentration standards, that spanned the concentration range of interest. Germanium was added to samples and standards to serve as the internal standard for normalization of analytical results. The uncertainty in measured Si and Al using this method is ±5%.

The pH was measured at experimental temperature on an unstirred aliquot of solution using a semi-micro 83-01 Orion Ross combination electrode. The reported accuracy is ±0.02 pH units (±4.5% in H+ activities), and the precision is ±0.10 pH units at pH ≈ 6.

2.5.1. Measuring Si isotopes in the spike solution and the inflow and outflow solutions

The isotopic composition of each sample of solution was measured twice: on the original sample and on a spiked aliquot of the sample. The first measurement was used in order to determine the isotopic composition of the solution while the second measurement was used to determine the silicon concentration using the isotope dilution method. In the following, the term "analytical spike" is used to describe the spiked solution that is used for the isotope dilution method, while the term "experimental spike" is used to refer to the spike that was used during the experiments. The "analytical spike" contained 189 μM Si with $^{29}Si/^{28}Si$ and $^{30}Si/^{28}Si$ ratios of 31.59 and 0.542, respectively. The spiked samples were prepared by mixing equal amounts of "analytical spike" solution and sample solution in a polyethylene bottle.

All samples were pretreated with cation exchange resin (AG 50W-X8 100–200 dry mesh size) before performing the isotopic analysis. This was done in order to reduce high concentrations of potassium and other cations that might interfere with the analysis. First, the resin was washed with 6 N HCl and then twice more with double distilled water. Then, for each sample, 0.2 g of the cation exchange resin was placed in a polyethylene bottle. Then, this measured amount of resin was washed with 1 ml of the sample. Afterward, 7 ml of the sample solution were placed in the same bottle with the treated resin. After mixing the solution with the resin for 1 h in a shaking water bath, the content was filtered through a Watman filter paper #1.

To verify the method, NBS28 and Big Batch were treated identically to samples. Isotope measurements of NBS28 and Big Batch provided identical ratios (within stated precision) for processed and unprocessed aliquots. The Si concentration, before and after the pretreatment, was measured with Perkin Elmer Lambda 2S spectrophotometer, using the Molybdate blue method (Koroleff, 1976). The results showed that there is no change in Si concentration within ±4%.

Isotopic ratios of Si of all solutions, including the inflow and the outflow solution that was used to spike the samples, were measured with a Thermo Neptune multi-collector inductively coupled plasma mass spectrometer (MC-ICP-MS) using standard-sample bracketing and Mg isotope normalization in "edge resolution mode" at the BRGM in Orleans, France. In this technique, a solution of known Mg isotope composition is added to both standards and samples, Si and Mg isotope ratios are measured simultaneously, the Si isotope ratios are corrected for mass discrimination proportionally to the Mg isotope adjustment

Table 1
Experimental conditions and results. The uncertainty (2σ) in measured Si and Al is ±5% and in measured isotopic ratios is ±0.02% (see Section 2.5).

No.	Time (h)	Al (μM)		Si (μM)		$^{29}Si/^{28}Si$		$^{30}Si/^{28}Si$	
		In	Out	In	Out	In	Out	In	Out
18	3619	0.056	0.716	189	195	0.09685	0.09607	0.03426	0.03445
24	3955	0.065	0.142	191	198	0.09695	0.09644	0.03426	0.03450
30	4292	0.079	0.141	199	199	0.09684	0.09649	0.03426	0.03453
36	4627	0.070	0.179	188	196	0.09695	0.09651	0.03428	0.03456
45	5131	0.067	1.550	201	199	0.09693	0.09533	0.03428	0.03426
54	5635	0.045	0.886	211	201	0.09585	0.09544	0.03426	0.03426
60	6140	0.070	0.754	198	200	0.09594	0.09522	0.03245	0.03425
64	6380	0.051	1.462	197	208	0.09592	0.09464	0.03426	0.03424

required assuming exponential mass dependent behavior, and Si isotope ratios of the samples are corrected by interpolation to adjusted values for the bracketing standards. Before the analysis, the samples were diluted with Teflon-distilled HCl to the concentration of 3% HCl, in order to match the sample matrix to the concentration and composition of the standard solution. The Si isotope standard NBS28 was used as the bracketing standard for all samples, and provides the zero point reference for the "delta scale". The secondary Si isotope standard "Big Batch" (Cardinal et al., 2003) was measured multiple times during the analytical session, giving an average $\delta^{30/28}Si_{NBS28}$ value of $-10.15‰$ which is in agreement with results obtained in other laboratories. The results of the measurements of the standards are presented in Table 2. The average uncertainty (2σ) in measured isotopic ratios using this method is $\pm 0.02\%$.

2.6. Error propagation

The present study compares reaction rates that were evaluated using various methods as is discussed below. For each calculation, uncertainty in rate was estimated using the Gaussian error propagation method (Barrante, 1974):

$$\Delta P = \left[\sum_i \left(\frac{\partial P}{\partial x_i}\right)^2 (\Delta x_i^2)\right]^{1/2} \quad (2)$$

where P is the calculated parameter (e.g., dissolution rate), and Δx_i is the estimated uncertainty in the measurements of x_i. The fully derived equation of each of the rate equations is presented in Electronic Annex EA-1.

3. RESULTS AND DISCUSSION

3.1. The proposed method

Traditional methods (henceforth, the "conventional method") use the change in concentration of the major ions (e.g., Si) that are released from the primary minerals to calculate dissolution rates. The accuracy and precision of the obtained rates are limited by the absolute analytical uncertainty of the concentration measurements. As noted by Ganor et al. (2007), the analytical challenge is to determine a small change in relatively high concentration. Therefore, improving the sensitivity of an analytical method does not help in improving the rate determination. The high precision of isotopic measurements enables the determination of the concentration of elements using the "isotope dilution" method.

The two major problems in measuring dissolution rates under close-to-natural conditions in laboratory experiments are (1) our inability to measure small differences in concentration between solutions with relatively high concentrations and (2) the inherent problem that the change in solution concentration is affected by both the dissolution of the primary mineral and the precipitation of the secondary mineral. The isotope dilution method improves the analytical ability but still measures the net change in concentration which is also affected by secondary mineral precipitation. To circumvent this problem, the novel method of the present study follows the change in isotopic ratio of a spiked solution during dissolution. Below, this method is demonstrated initially for a generic flow-through experiment and thereafter for a batch experiment.

3.1.1. Flow-through experiments

The change in concentration of the dissolved mineral's products (e.g., silicon) in a flow-through system (Lasaga, 1998) may be described by the following mass balance:

$$\frac{dC_i}{dt} = -\frac{q}{V}\cdot(C_{i,out} - C_{i,inf}) + \upsilon_{i,dis}\cdot\frac{A_{dis}}{V}\cdot R_{dis} \quad (3)$$

where R_{dis} is the dissolution rate (mol m^{-2} s^{-1}), $C_{i,inf}$ and $C_{i,out}$ are the concentrations of component i in the inflow and outflow solutions, respectively (mol L^{-1}); t is time (s); A_{dis} is surface area of the dissolving mineral (m^2); $\upsilon_{i,dis}$ is stoichiometric coefficient of i in the dissolution reaction; q is fluid flux through the system (L s^{-1}); and V is the volume of the flow-through reaction cell (L).

The dissolution rate of the mineral can be determined by rearranging Eq. (3):

$$\upsilon_{i,dis}\cdot R_{dis} = \frac{dC_i}{dt}\cdot\frac{V}{A_{dis}} + \frac{q}{A_{dis}}\cdot(C_{i,out} - C_{i,inf}) \quad (4)$$

The dissolution rate in such an experiment may be readily obtained if steady state is reached, i.e., if the composition of the solution becomes constant with time ($\frac{dC_i}{dt} = 0$). In this case, dissolution rate is balanced by the difference in concentration between inflow and outflow solutions:

$$\upsilon_{i,dis}\cdot R_{dis} = \frac{q}{A_{dis}}\cdot(C_{i,out} - C_{i,inf}) \quad (5)$$

Table 2
Isotopic ratios of the silicon standard solutions as measured with MC-ICP-MS.

NBS28	Time (h)	$^{29}Si/^{28}Si$ normalized	$^{30}Si/^{28}Si$ normalized	Big Batch	Time (h)	$^{29}Si/^{28}Si$	$^{29}Si/^{28}Si$
Replicate 1	130,210	0.05048	0.03331	Replicate 1	1307,47	0.05023	0.03296
Replicate 2	141,840	0.05049	0.03331	Replicate 2	142,448	0.05023	0.03698
Replicate 3	145,742	0.05048	0.03331	Replicate 3	150,348	0.05022	0.03297
Replicate 4	160,941	0.05049	0.03331	Replicate 4	161,501	0.05022	0.03298
Average		0.05049	0.03331	Average		0.5023	0.03297
STDEV		4.95E-06	2.33E-06	STDEV		4.89E-06	5.90E-06
RSD%		0.0098	0.007	RSD%		0.0097	0.018
				Relative to NBS28 (‰)		−5.147	−10.157

The precision of most standard analytical methods for the determination of the concentration of major ions are of the order of few percent. This precision is much larger than the expected relative differences between the inflow and the outflow of a theoretical flow-through experiment that simulate natural conditions (Ganor et al., 2007). By using isotope dilution it is possible to significantly improve the precision.

In the isotope dilution method, "analytical spike solutions" with known silicon concentration and isotopic composition are added to samples with unknown concentration of silicon (e.g., inflow and outflow solutions in flow-through experiment or any solution during a batch experiment). When mixing the two solutions in a known amount, it is possible to use the measured isotopic ratio of the mixture in order to calculate the original concentration of a sample (c_{samp}) as follows:

$$C_{samp} = \frac{C_{spike} \cdot \left(\left(\frac{^{29}Si}{^{total}Si}\right)_{spike} \cdot X - \left(\frac{^{28}Si}{^{total}Si}\right)_{spike} \cdot X \cdot \left(\frac{^{29}Si}{^{28}Si}\right)_{mix} \right)}{(1-X) \cdot \left(\left(\frac{^{28}Si}{^{total}Si}\right)_{samp} \cdot \left(\frac{^{29}Si}{^{28}Si}\right)_{mix} - \left(\frac{^{29}Si}{^{total}Si}\right)_{samp} \right)} \tag{6}$$

where ^{i}Si and ^{total}Si are the amounts of the silicon isotope i, and the total amount of all the silicon isotopes (moles), respectively; C_j is silicon concentrations in solution j; the subscripts *samp, spike* and *mix* refer to the sample, the added analytical spiked solution, and the resulting mixture of the two; and X is the relative mass of the analytical spiked solution.

The dissolution rate at steady state may be determined by substituting the silicon concentrations in the inflow and outflow solutions, calculated with Eq. (6), into Eq. (5). This will reduce the uncertainty in rate calculations. The hidden assumption in calculating the rate using Eq. (5) is that the only source and sink of i is from the dissolution reaction. However, as mentioned above, under close to natural conditions, the resulting rate will be the net rate of silicon release by dissolution minus its consumption by precipitation. Taking into account the effect of precipitation of secondary minerals, Eq. (5) should be rewritten as:

$$\upsilon_{i,dis} \cdot R_{dis} \cdot A_{dis} + \upsilon_{i,pre} \cdot R_{pre} \cdot A_{pre} = q \cdot (C_{i,out} - C_{i,inf}) \tag{7}$$

where R_{pre} is the precipitation rate (mol m^{-2} s^{-1}); A_{pre} is the surface area of the precipitated mineral (m^2); and $\upsilon_{i,pre}$ is the stoichiometric coefficient of i in the precipitation reaction. Note that in our formalism, the rate is defined to be negative for precipitation and positive for dissolution, and hence the precipitation term is added to the dissolution term.

In order to calculate the overall dissolution rate, we suggest performing the experiment with inflow solutions that contains isotopic spike (henceforth, "experimental spike"). Due to the difference between the isotopic composition of the inflow and that of the dissolving mineral, the dissolution rate may be determined by following the isotopic composition of the outflow. The main assumption in the following calculations is that fractionation during albite dissolution and precipitation of a secondary mineral is negligible. From previous studies (e.g., Douthitt, 1982; De La Rocha et al., 2000) it seems that there might be a certain amount of fractionation during the precipitation of clay minerals. The effect of such fractionation on the obtained rate will be examined in Section 3.3 below.

Using the assumption that fractionation is negligible, the steady-state mass balance of ^{28}Si may be calculated using equations similar to Eq. (7):

$$\left(\frac{^{28}Si}{^{total}Si}\right)_{dis} \cdot R_{dis} \cdot \upsilon_{dis} \cdot A_{dis} + \left(\frac{^{28}Si}{^{total}Si}\right)_{out} R_{pre} \cdot \upsilon_{pre} \cdot A_{pre} = q \cdot \left(\left(\frac{^{28}Si}{^{total}Si}\right)_{out} \cdot C_{Si,out} - \left(\frac{^{28}Si}{^{total}Si}\right)_{inf} \cdot C_{Si,inf} \right) \tag{8}$$

Rearranging Eq. (8) gives:

$$^{28}Si_{out} \cdot \frac{(q \cdot C_{Si,out} - R_{pre} \cdot \upsilon_{pre} \cdot A_{pre})}{^{total}Si_{out}} = \left(\frac{^{28}Si}{^{total}Si}\right)_{dis} \cdot R_{dis} \cdot \upsilon_{dis} \cdot A_{dis} + q \cdot \left(\frac{^{28}Si}{^{total}Si}\right)_{inf} \cdot C_{Si,inf} \tag{9}$$

Dividing similar equation for ^{29}Si by Eq. (9) gives:

$$\left(\frac{^{29}Si}{^{28}Si}\right)_{out} = \frac{\left(\frac{^{29}Si}{^{total}Si}\right)_{dis} \cdot R_{dis} \cdot \upsilon_{dis} \cdot A_{dis} + q \cdot \left(\frac{^{29}Si}{^{total}Si}\right)_{\inf} \cdot C_{Si,inf}}{\left(\frac{^{28}Si}{^{total}Si}\right)_{dis} \cdot R_{dis} \cdot \upsilon_{dis} \cdot A_{dis} + q \cdot \left(\frac{^{28}Si}{^{total}Si}\right)_{\inf} \cdot C_{Si,inf}} \tag{10}$$

The real dissolution rate of the mineral (without the effect of precipitation) is obtained by rearranging Eq. (10):

$$R_{dis} = \frac{q}{\upsilon_{dis} \cdot A_{dis}} \frac{\left(\frac{^{29}Si}{^{total}Si}\right)_{inf} \cdot C_{Si,inf} - \left(\frac{^{29}Si}{^{28}Si}\right)_{out} \cdot \left(\frac{^{28}Si}{^{total}Si}\right)_{inf} \cdot C_{Si,inf}}{\left(\frac{^{29}Si}{^{28}Si}\right)_{out} \cdot \left(\frac{^{28}Si}{^{total}Si}\right)_{dis} - \left(\frac{^{29}Si}{^{total}Si}\right)_{dis}} \tag{11}$$

The above method will be regarded in the present study as the "isotope ratio method". In contrast to the "isotope dilution method", the calculated reaction rate with the "isotope ratio method" is influenced only by the dissolution of the primary silicate minerals. The precipitation of silicate minerals changes the silicon concentration in the outflow solution but not the isotopic composition.

The precipitation rate of the secondary mineral (R_{pre}) may be calculated by subtracting the release rate of Si that was calculated using the isotope dilution method ($R_{dis,id}$) from the rate that was the isotope ratio method ($R_{dis,ir}$):

$$R_{pre} \cdot A_{pre} = -\frac{(R_{dis,ir} - R_{dis,id}) \cdot \upsilon_{i,dis} \cdot A_{dis}}{\upsilon_{i,pre}} \tag{12}$$

3.1.2. Batch experiment

The change in concentration of the dissolved mineral's products in a batch reactor may be described by the following mass balance:

$$\frac{dC_i}{dt} = \upsilon_{i,dis} \cdot \frac{A_{dis}}{V} \cdot R_{dis} \tag{13}$$

where C_i is the concentrations of component i in the reactor (mol L^{-1}); t is time (s); and V is the volume of the batch reactor (L). Rearranging Eq. (13) gives:

$$R_{dis} \cdot \upsilon_{i,dis} = \frac{dC_j}{dt} \cdot \frac{V}{A_{dis}} \tag{14}$$

Typically, the dissolution rate in a batch experiment is obtained by measuring the concentration of a component i at different times during the experiment and using Eq. (14). The hidden assumption in this calculation is that the change in concentration (ΔC_i) is linear with time during the sampling interval, and therefore the reaction rate may be readily calculated by substituting the average change in concentration with time ($\Delta C_i/\Delta t$) for the time derivative of the concentration (dC_i/dt) in Eq. (14).

As in the case of the flow-through reactor, if i is removed by precipitation of secondary phases, the resulting rate is the net rate of the release of i by dissolution minus its consumption by precipitation. Taking into account the effect of precipitation of secondary minerals, Eq. (13) should be rewritten as:

$$\frac{dC_i}{dt} = \frac{\upsilon_{i,dis} \cdot A_{dis} \cdot R_{dis} + \upsilon_{i,pre} \cdot A_{pre} \cdot R_{pre}}{V} \tag{15}$$

The net dissolution rate of a silicate mineral may be obtained by performing batch experiment with initial solution that contains experimental spike. Again, it is assumed that fractionation during the dissolution of the primary mineral and precipitation of the secondary mineral is negligible. The mass balances of the amounts (moles) of Si, ^{28}Si and ^{29}Si in the solution are:

$$\frac{dSi}{dt} = \upsilon_{Si,dis} \cdot A_{dis} \cdot R_{dis} + \upsilon_{Si,pre} \cdot A_{pre} \cdot R_{pre} \tag{16}$$

$$\frac{d^{28}Si}{dt} = \upsilon_{Si,dis} \cdot A_{dis} \cdot R_{dis} \cdot \left(\frac{^{28}Si}{^{total}Si}\right)_{dis} + \upsilon_{Si,pre} \cdot A_{pre} \cdot R_{pre} \cdot \left(\frac{^{28}Si}{^{total}Si}\right)_{t} \tag{17}$$

$$\frac{d^{29}Si}{dt} = \upsilon_{Si,dis} \cdot A_{dis} \cdot R_{dis} \cdot \left(\frac{^{29}Si}{^{total}Si}\right)_{dis} + \upsilon_{Si,pre} \cdot A_{pre} \cdot R_{pre} \cdot \left(\frac{^{29}Si}{^{total}Si}\right)_{t} \tag{18}$$

where the subscript t refers to the solution at time t. Rearranging Eqs. (17) and (18) gives,

$$\left(\frac{^{28}Si}{^{total}Si}\right)_{t} = \frac{\frac{d^{28}Si}{dt} - \upsilon_{Si,dis} \cdot A_{dis} \cdot R_{dis} \cdot \left(\frac{^{28}Si}{^{total}Si}\right)_{dis}}{\upsilon_{Si,pre} \cdot A_{pre} \cdot R_{pre}} \tag{19}$$

$$\left(\frac{^{29}Si}{^{total}Si}\right)_{t} = \frac{\frac{d^{29}Si}{dt} - \upsilon_{Si,dis} \cdot A_{dis} \cdot R_{dis} \cdot \left(\frac{^{29}Si}{^{total}Si}\right)_{dis}}{\upsilon_{Si,pre} \cdot A_{pre} \cdot R_{pre}} \tag{20}$$

Dividing Eq. (20) by Eq. (19) gives the ^{29}Si/^{28}Si ratio at time t:

$$\left(\frac{^{29}Si}{^{28}Si}\right)_{t} = \frac{\frac{d^{29}Si}{dt} - \upsilon_{Si,dis} \cdot A_{dis} \cdot R_{dis} \cdot \left(\frac{^{29}Si}{^{total}Si}\right)_{dis}}{\frac{d^{28}Si}{dt} - \upsilon_{Si,dis} \cdot A_{dis} \cdot R_{dis} \cdot \left(\frac{^{28}Si}{^{total}Si}\right)_{dis}} \tag{21}$$

The dissolution rate may be obtained by rearranging Eq. (21):

$$R_{dis} = \frac{\left(\frac{^{29}Si}{^{28}Si}\right)_{t} \cdot \frac{d^{28}Si}{dt} - \frac{d^{29}Si}{dt}}{\left(\left(\frac{^{29}Si}{^{28}Si}\right)_{t} \cdot \left(\frac{^{28}Si}{^{total}Si}\right)_{dis} - \left(\frac{^{29}Si}{^{total}Si}\right)_{dis}\right) \cdot \upsilon_{Si,dis} \cdot A_{dis}} \tag{22}$$

Precipitation rate can be calculated by rearranging Eq. (16) and substituting the change of silicon with time that is measured with the isotope dilution method (Eq. (6)) and the albite dissolution rate which was determined using the isotope ratio method (Eq. (22)):

$$R_{pre} = \frac{\frac{dSi}{dt} - \upsilon_{Si,dis} \cdot A_{dis} \cdot R_{dis}}{\upsilon_{Si,pre} \cdot A_{pre}} \tag{23}$$

3.2. Simulations without isotopic fractionation

In order to demonstrate the benefits of the proposed method to measure simultaneously two parallel slow rate reactions (dissolution of primary mineral and precipitation of secondary mineral), simulations of a flow-through and batch experiments have been conducted. The input parameters of each of the simulations and their uncertainties are presented in Table 3. In all the simulations albite ($NaAlSi_3O_8$) was dissolved and kaolinite ($Al_2Si_2O_5(OH)_4$) was precipitated. Albite dissolution was simulated using the rate law of Burch et al. (1993):

$$Rate_{diss} = k_1(1 - e^{(-8.4 \cdot 10^{-17} \cdot (\Delta G/RT)^{15})}) + k_2(1 - e^{(\Delta G/RT)^{1.45}}) \tag{24}$$

where k_1 and k_2 are rate coefficients that depend on the environmental conditions. At 80 °C, pH 8.8 using a freshly ground Amelia albite $k_1 = 30.46 \times 10^{-12}$ and $k_2 = 2.73 \times 10^{-12}$ mol m^{-2} s^{-1} (Burch et al., 1993). Assuming activation energy of 15 kcal/mol, the rate coefficients at 25 °C were calculated to be $k_1 = 5.89 \times 10^{-13}$ and $k_2 = 5.28 \times 10^{-14}$ mol m^{-2} s^{-1}. Following the reasoning of Ganor et al. (2007), kaolinite precipitation was simulated using a rate law that include the prediction of transition state theory for the rate dependence on deviation from equilibrium:

$$Rate_{precip} = k_p(1 - e^{(\Delta G/RT)}) \tag{25}$$

Applying the principle of detailed balancing, k_p is equal to the far-from-equilibrium dissolution rate. This method was confirmed for quartz dissolution and precipitation at 180 °C and pH 4 (Ganor et al., 2005). In the present study simulations, a k_p value of 3×10^{-13} mol m^{-2} s^{-1} was chosen based on the far from equilibrium dissolution rate of kaolinite at 25 °C and pH ~6.5 which were determined in laboratory experiments by Wieland and Stumm (1992).

3.2.1. Simulation of flow-through experiment

The following conditions were used for the first flow-through simulation: 0.5 g of albite with specific surface area of 0.39 m^2 g^{-1} is dissolved in a 200 ml flow-through reactor with flux of 7.33×10^{-8} L s^{-1} of inflow solution containing 50 μM Si with isotopic composition of 0.04% ^{28}Si, 99.9% ^{29}Si and 0.06% ^{30}Si, 4 μM Al, 10 μM Na, and pH 4.01. This inflow solution is under saturated with respect to albite ($\Omega = 4.3 \times 10^{-11}$) and over saturated with respect to kaolinite ($\Omega = 1.48$). Assuming that kaolinite is the only secondary phase that precipitated, the changes in concentrations and isotopic compositions are controlled by albite dissolution and kaolinite precipitation.

In this simulation, only the steady state stage of the experiment was simulated. It was assumed that after less than three residence times the experiment was at steady state in which albite is dissolved, kaolinite is precipitated and the composition of the outflow solution is constant. We further assume for simplicity that the mass of the albite

Table 3
Simulations input parameters.

Input parameters	Section 3.2.1: flow-through	Sections 3.2.2 and 3.3.2: batch and batch with fractionation	Section 3.3.1: flow-through with fractionation-1	Section 3.3.1: flow-through with fractionation-2	Section 3.3.1: flow-through with fractionation-3	Section 3.3.1:flow-through with fractionation-4	Section 3.3.1: flow-through with fractionation-5	Section 3.3.1: flow-through with fractionation-6	Uncertainty (2 s.d.)
pH	4.014	5	4.014	4.014	4.014	4.014	4.014	4.014	±0.1
Al (μM)	4	0	4	4	4	4	4	4	5%
Si (μM)	50	40	50	Variable	50	50	50	50	4%[a], 0.05%[b]
Na (μM)	10	5	10	10	10	10	10	10	5%
Albite mass (g)	0.5	0.5	0.5	0.5	0.5	0.5	0.5	0.5	±0.0001
Albite specific surface area ($m^2\ g^{-1}$)	0.39	0.13	0.39	0.39	0.39	0.39	0.39	0.39	10%
Albite dissolution rate ($mol\ m^{-2}\ s^{-1}$)	6×10^{-13}	Burch rate law	6×10^{-13}	6×10^{-13}	6×10^{-13}	Variable	6×10^{-13}	6×10^{-13}	
Burchrate law k_1 ($mol\ m^{-2}\ s^{-1}$)	–	5.8895×10^{-13}	–	–	–	–	–	–	*
Burchrate law k_2 ($mol\ m^{-2}\ s^{-1}$)	–	5.2787×10^{-14}	–	–	–	–	–	–	*
Activation energy (kCal)	–	15	–	–	–	–	–	–	*
Kaolinite mass (g)	0.04587	0.00040299[c]	0.04587	0.04587	0.04587	0.04587	0.04587	0.04587	0.0001
Kaolinite specific surface area ($m^2\ g^{-1}$)	21.8	Change in time	21.8	21.8	21.8	21.8	21.8	21.8	10%
Kaolinite precipitation rate ($mol\ s^{-1}$)	-7.86×10^{-14}	Change in time	-7.86×10^{-14}	-7.86×10^{-14}	-7.86×10^{-14}	-7.86×10^{-14}	Variable	-7.86×10^{-14}	
kaolinite precipitation rate ($mol\ m^{-1}\ s^{-1}$)	-7.86×10^{-14}	TST rate law	-7.86×10^{-14}	-7.86×10^{-14}	-7.86×10^{-14}	-7.86×10^{-14}	Variable	-7.86×10^{-14}	
Kaolinite rate constant ($mol\ m^{-2}\ s^{-1}$)	–	3×10^{-13}	–	–	–	–	–	–	*
^{28}Si in solution	0.04%	0.04%	0.04%	0.04%	0.04%	0.04%	0.04%	Variable	0.001%
^{29}Si in solution	99.90%	99.90%	99.90%	99.90%	99.90%	99.90%	99.90%	Variable	0.02%
^{30}Si in solution	0.06%	0.06%	0.06%	0.06%	0.06%	0.06%	0.06%	Variable	0.07%
^{28}Si out solution	8.10%	–							0.001%
^{29}Si out solution	91.58%	–							0.02%
^{30}Si out solution	0.32%	–							0.07%
Temperature	25 °C	25 °C	25 °C	25 °C	25 °C	25 °C	25 °C	25 °C	*
q ($L\ s^{-1}$)	7.33×10^{-8}	–	7.33×10^{-8}	7.33×10^{-8}	Variable	7.33×10^{-8}	7.33×10^{-8}	7.33×10^{-8}	6.38%
Solution mass (g)	–	200	–	–	–	–	–	–	±0.01
Ω Albite in	4.3×10^{-11}	–	4.3×10^{-11}	4.3×10^{-11}	4.3×10^{-11}	4.3×10^{-11}	4.3×10^{-11}	4.3×10^{-11}	*

(*continued on next page*)

Table 3 (*continued*)

Input parameters	Section 3.2.1: flow-through	Sections 3.2.2 and 3.3.2: batch and batch with fractionation	Section 3.3.1: flow-through with fractionation-1	Section 3.3.1: flow-through with fractionation-2	Section 3.3.1: flow-through with fractionation-3	Section 3.3.1:flow-through with fractionation-4	Section 3.3.1: flow-through with fractionation-5	Section 3.3.1: flow-through with fractionation-6	Uncertainty (2 s.d.)
Ω Albite out	1.15×10^{-10}	–	1.15×10^{-10}	1.15×10^{-10}	1.15×10^{-10}	1.15×10^{-10}	1.15×10^{-10}	1.15×10^{-10}	*
Ω Kaolinite in	1.48	–	1.48	1.48	1.48	1.48	1.48	1.48	*
Ω Kaolinite out	1.26	–	1.26	1.26	1.26	1.26	1.26	1.26	*
log *k* Albite	2.065	2.065	2.065	2.065	2.065	2.065	2.065	2.065	*
log *k* Kaolinite	4.501	4.501	4.501	4.501	4.501	4.501	4.501	4.501	*
Parameter that was varied during the simulation	–	–	Fractionation factors	Si concentration	Flow rate	Albite dissolution rate	Kaolinite precipitation rate	$^{29}Si/^{28}Si$	

[a] Conventional method.
[b] Isotope dilution.
[c] Mass in the end of simulation, initial mass = 0.
[*] Uncertainty was not introduced into the simulation.

(0.5 g) and kaolinite (0.0459 g) and their specific surface areas (0.39 and 21.8 m^2/g, respectively) remain constant and that their dissolution and precipitation rates are therefore constant and equal 6×10^{-13} and 7.86×10^{-14} mol m^{-2} s^{-1}, respectively (1.17×10^{-13} and 7.86×10^{-14} mol s^{-1}). To simulate the analytical uncertainty, an error, which was randomly selected from a normal distribution of errors of ±2% (one standard deviation), was added to the value of each of the ion concentrations of all inflow and outflow. Similarly, an error of ±0.01% (one standard deviation) was added to the values of the isotopic ratios. The NORM.INV functions of Microsoft® Office Excel 2010, was used to simulate the normal distribution, and the RAND function was used to randomly select the probability.

The change with time in the simulated concentration is shown in Fig. 1. The error bars (±4%) represent two standard deviations (2 s.d.). The Si and Na concentrations of the outflow solution are higher and that of Al is lower than those of the inflow solution, due to albite dissolution and kaolinite precipitation. However, in most cases these differences are within analytical uncertainties. In contrast, due to the lower analytical uncertainty associated with the determination of Si using the isotope dilution method (≈±0.05%, 2s.d.), a significant change between the inflow and the outflow concentration may be observed (Fig. 2). A parallel significant difference is observed in the isotopic ratio of the outflow (Fig. 3).

Using the simulated observations, the steady-state dissolution rate of albite was calculated using the three methods (Eqs. (5), (6) and (11)). The uncertainty in the rate that was calculated using the isotope dilution method is significantly smaller than that in the rate that was calculated using the conventional method (Fig. 4). The relative uncertainties of the rates that were calculated using the isotope dilution method are similar to those that were calculated using the isotope ratio method. However, as the absolute rate of the former is about half than the latter, the absolute uncertainty of the rates are significantly different. Due to the large uncertainty, the rate that was calculated using the conventional method is not significantly different from zero in most of the samples, and within uncertainty may even represent albite precipitation (Figs. 4 and 5a), which is not reasonable thermodynamically, as the solution is undersaturated with respect to albite ($\Omega = 1.15 \times 10^{-10}$). Rates calculated using the conventional method and the isotope dilution method are slower than the "actual" dissolution rate (Fig. 5a), due to the assumption in Eq. (5) that the change in Si concentration is solely due to albite dissolution. Dissolution rates, calculated using isotope ratio, agree with the "actual" dissolution rate as the steady-state isotopic ratio is not influenced by kaolinite precipitation. Kaolinite precipitation rate (Fig. 5b) was calculated by subtracting the release rate of Si that was calculated using the isotope dilution method ($R_{dis,id}$) from the rate that was the isotope ratio method (Eq. (12)). Within uncertainty, the calculated precipitation rate is equal the actual rate (Fig. 5a).

The albite dissolution rate in the present simulation was 6×10^{-13} mol m^2 s^{-1}, and the release rate of Si was

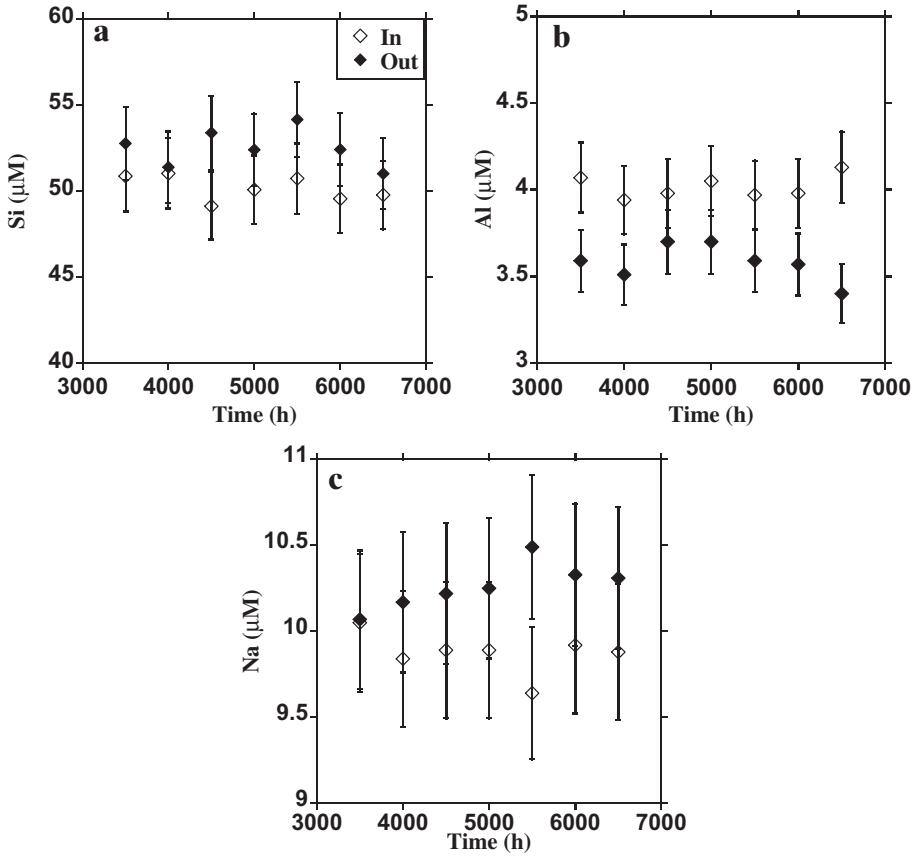

Fig. 1. The change with time in the simulated concentrations of Si (a), Al (b) and Na (c) in a simulation of a flow-through experiment. The simulation conditions are described in Section 3.2.1. Error bars represent the simulated uncertainty (±2 s.d.).

3.5×10^{-13} mol s^{-1}. Under this condition, with Si concentration in the inflow solution of 50 μM and $^{29}Si/^{28}Si$ ratio of about 2500, there is a large change in the isotopic composition due to dissolution and therefore the uncertainty in measuring the isotopic ratios does not have a significant effect on the uncertainty of the dissolution rate, which is controlled by uncertainties in the determination of the surface area. Decreasing dissolution rate will decrease the change in isotopic ratio, but as long as the change in isotopic ratio is significantly larger than the analytical uncertainty, it is possible to accurately measure the rate. To evaluate the limits of the proposed method, a series of simulations was conducted with conditions identical to those in the basic simulation but with different dissolution rates. In this series of simulations, it was assumed that the analytical uncertainty of the measurements of the isotopic ratio using the MC-ICP-MS is 0.1%. Fig. 6a shows that the proposed method can determine albite dissolution rates of 5×10^{-17} mol m^2 s^{-1} with small uncertainty. The uncertainty increases to 50% for rates of 1×10^{-17} mol m^2 s^{-1}. For dissolution rates equal or slower than 4×10^{-18} mol m^2 s^{-1} the uncertainties exceeds 100%. As will be discussed below (Section 4), the proposed method can determine the entire range of plagioclase dissolution rate in the field (shaded area in Fig. 6a). It is important to note that the level of the isotopic enrichment of the inflow solution strongly affect the uncertainty in the rate measurements. While for relatively faster rates (e.g., 6×10^{-13} mol m^2 s^{-1}), a reasonable uncertainty may be obtained by using inflow with $^{29}Si/^{28}Si$ of about 0.1, a highly enriched inflow with $^{29}Si/^{28}Si$ of more than 1000 is needed for the slowest rates observed in the field (Fig. 6b).

3.2.2. Simulation of batch experiment

In this simulation, 0.5 g of albite was dissolved in 200 g of solution in a batch reactor. Initially the solution contains 40 μM Si with the same isotopic composition as in the above simulation of flow-through experiment. The solution has an initial pH of 5 and a Na concentration of 5 μM. No Al was added. The rates of albite dissolution and kaolinite precipitation were calculated using the rate laws of Eqs. (24) and (25). The change in the concentrations of the elements and of the isotopic compositions of Si with time due to albite dissolution and kaolinite precipitation was simulated using a forward model that solves Eqs. (16), (17) and (18) and the rate laws of Eqs. (24) and (25), assuming no isotopic fractionation. At the end of each increment of the model the decrease in albite mass was recorded. Albite surface area (A_t) following dissolution was related to the initial surface area (A_i) assuming that the dissolution rates on all faces are equal (i.e., that the shape of the crystals remains unchanged):

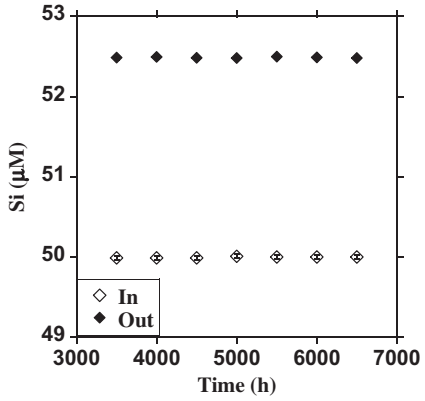

Fig. 2. The change with time in the simulated concentrations of Si, which were derived based on the isotope dilution method, in a simulation of a flow-through experiment. The simulation conditions are described in Section 3.2.1. Error bars represent the simulated uncertainty (±2 s.d.).

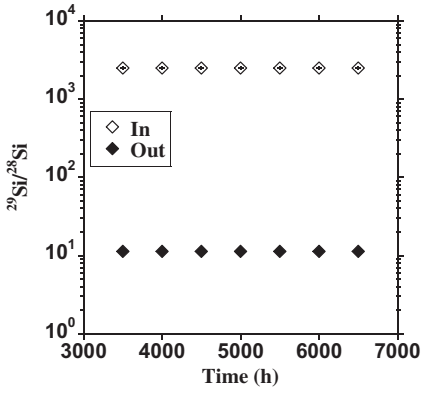

Fig. 3. The change with time in the simulated $^{29}Si/^{28}Si$ ratio in a simulation of a flow-through experiment. The simulation conditions are described in Section 3.2.1. The error bars (±2 s.d.) are smaller than the size of the symbols.

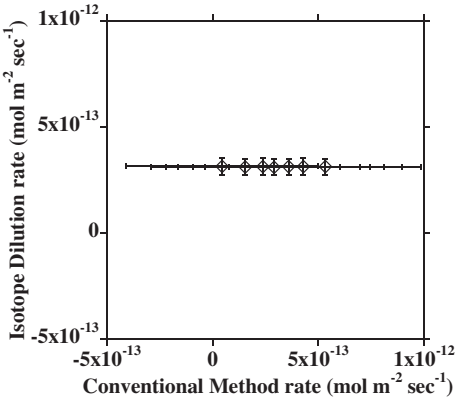

Fig. 4. A comparison of the steady-state dissolution rates that were calculated using the isotope dilution method to the rates that were calculated using the conventional method in a simulation of flow-through experiments. Error bars represent the propagated uncertainties (±2 s.d.) of the calculated rates.

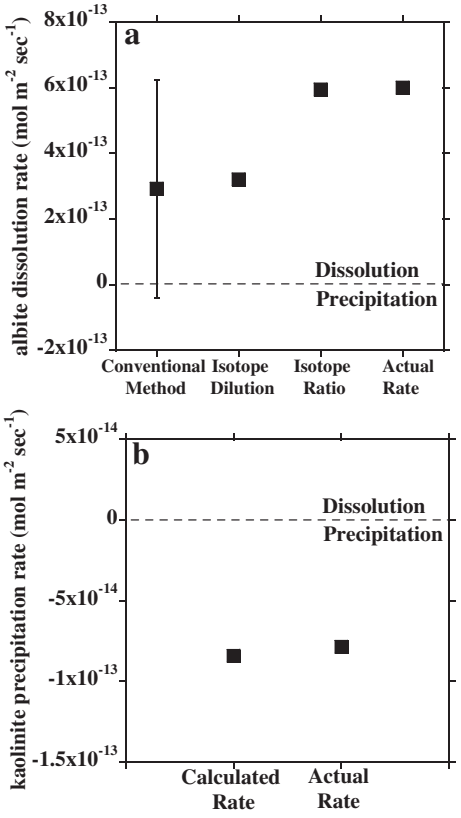

Fig. 5. (a) Comparison of the average dissolution rates at steady state that were retrieved from the simulated concentrations and isotopic composition of flow-through experiments using the three different methods to the "actual" simulated rate. (b) Comparison of the average kaolinite precipitation rate at steady state that was retrieved from the simulated concentrations and isotopic composition of flow-through experiments to the "actual" simulated rate. Error bars represent two standard deviations of the mean rate.

$$A_t = A_i \cdot \left(\frac{M_t}{M_{(i)}}\right)^{2/3}, \tag{26}$$

where A and M are surface area (m^2) and mass (g) of the albite, respectively, and the subscripts i and t refer to the initial time and any other time point of the simulation, respectively. It is important to note that in the real world, changes in surface area may be more complex. The reactive surface areas may also vary during experiments as a result of the extinction of highly reactive fine particles (Helgeson et al., 1984), change of the ratios of reactive and nonreactive sites (Gautier et al., 2001), mechanical disaggregation of particles (Nagy and Lasaga, 1992; Ganor et al., 1999), and formation of surface coating (Ganor et al., 1995; Nugent et al., 1998; Cubillas et al., 2005; Metz et al., 2005). However, as the goal of the present study is to describe and examine the proposed isotope ratio method, simulation of these possible changes in the reactivity of the dissolved mineral is beyond the scope of the present study.

Initially, the solution was undersaturated with respect to kaolinite. Due to albite dissolution the solution became oversaturated 17 h after the experiment began. For simplicity, the simulation ignores nucleation and assumes that as

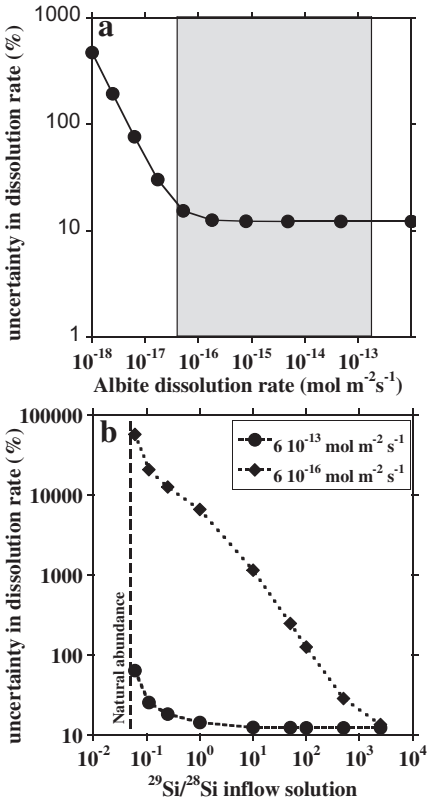

Fig. 6. (a) The effect of dissolution rate on the analytical uncertainty (%) in albite dissolution rates that were derived from simulated flow-through experiments using the isotope ratio method. The shaded area represents the reported range of field-based dissolution rates (according to White and Brantley, 2003). (b) The effect of the spike enrichment level ($^{29}Si/^{28}Si$) on the analytical uncertainty for different dissolution rates.

the solution becomes over saturated with respect to kaolinite, an initial amount of reactive kaolinite was introduced with surface area of 1 m^2. During the duration of the simulation, 0.4 mg kaolinite was precipitated. As the maximum contribution of the precipitating kaolinite to the surface area is less than 2%, it was assumed that the reactive surface area of the kaolinite remains constant throughout the simulation.

The change in solution's chemistry during the simulation of the batch experiment is shown in Fig. 7. As the simulation progressed, the sampling frequency was reduced logarithmically, and each time interval between two samples was 25% longer than the previous time interval. As in the above flow-through simulation, errors of ±2%, ±0.01% and 0.05 units (one standard deviation), which were randomly selected from a normal distribution, were added to the value of each of the ions concentrations, the isotopic ratios and pH, respectively. Only after more than one month, the measured Si concentration is significantly different from the initial concentration. Due to the strong contrast between the initial isotopic composition of the solution and the isotopic composition of the dissolved albite, the $^{29}Si/^{28}Si$ ratio is very sensitive to dissolution and a significant change in this ratio is observed within less than a day. Dissolution rates were initially calculated using the conventional method and the isotope dilution method. The time derivative of the concentration (dC/dt in Eq. (14)) was approximated based on the slope of the change in Si concentration with time between each three successive samples. The dissolution rates calculated during the first month of the simulation, using the conventional method, represent only the "analytical noise" that was introduced to the simulation, and are therefore meaningless (Fig. 8). Significant rates were calculated only when a change over more than a month was recorded. The rates that were calculated using the isotope dilution method had lower scatter and are significant when a change over more than one day was recorded. Due to the precipitation of the kaolinite, neither method succeeds at reconstructing the actual albite dissolution rate, which stays nearly constant during the simulation (inset in Fig. 8). In contrast, after less than a day, rates calculated using the isotope ratio method reconstruct the albite dissolution rates very well and with relatively small uncertainties (Fig. 8). Kaolinite precipitation rates were also reconstructed successfully, but only when the calculated release rate of Si via the isotope dilution was significant, i.e., after the first few days of the simulation (Fig. 9).

3.3. Simulating the effect of isotope fractionation

The proposed method is using the assumption that there is no fractionation during kaolinite precipitation. However, this assumption is probably wrong (e.g., Douthitt, 1982; De La Rocha et al., 2000). The fractionation may be described by a fractionation factor, which is defined as:

$$\alpha = \frac{\left(\frac{d^{29}Si/dt}{d^{28}Si/dt}\right)_{Ka}}{\left(\frac{^{29}Si}{^{28}Si}\right)_{sol}} \quad (27)$$

where d^iSi/dt is the incorporation rate (mol s^{-1}) of isotope i on the surface of the solid (kaolinite in the present study), and the subscript *sol* refers to the solution. For convenience, the fractionation is described in the present study using the ε (epsilon) notation were

$$\varepsilon = 1000(\alpha - 1) = 1000\left(\frac{\left(\frac{d^{29}Si/dt}{d^{28}Si/dt}\right)_{Ka}}{\left(\frac{^{29}Si}{^{28}Si}\right)_{sol}} - 1\right) \quad (28)$$

In order to simulate fractionation, an isotopic exchange reaction was added to each time step of the model:

$$^{29}Si_{sol} + {}^{28}Si_{Ka} \leftrightarrow {}^{28}Si_{sol} + {}^{29}Si_{Ka} \quad (29)$$

Providing that the total precipitation rate is constant, if the rate of one isotope (relative to its abundance) is faster than the total rate, the rate of the other isotope should be slower so the mass balance will be in maintain. Therefore, mathematically, the fractionation may be described using an isotopic exchange reaction. It is important to note that Eq. (29) is not a mechanistic equation, it is used solely as a mathematical construct to allow for a differential rate of precipitation of the different isotopes without affecting the total precipitation rate.

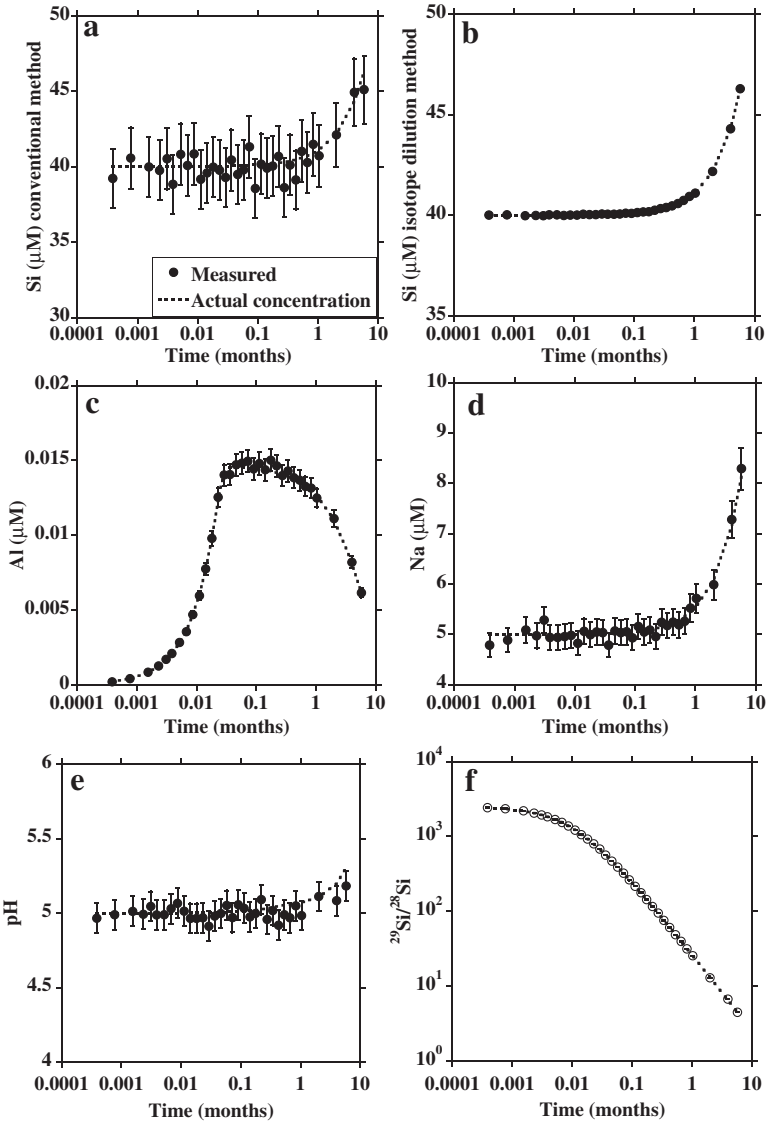

Fig. 7. The change with time in the simulated concentrations of Si which were derived using a standard analytical method (a), isotope dilution method (b), concentrations of Al (c), concentrations of Na (d), pH (e), and $^{29}Si/^{28}Si$ ratio (f) in a simulation of a batch experiment. The dashed lines represent the "actual" simulated values. The simulation conditions are described in Section 3.2.2. Error bars represent the simulated uncertainty (±2 s.d.).

This approach was used to simulate the change with time in Si concentrations and in its isotopic composition in flow-through and batch experiments in which albite was dissolved and kaolinite was precipitated with isotopic fractionations with epsilon values of 0.5–20‰ (α equals 1.0005–1.02).

The mass balance of ^{28}Si and ^{29}Si on the surface of the kaolinite with isotopic fractionation is described by:

$$\left(\frac{d^{28}Si}{dt}\right)_{Ka} = -R_{Ex} - \frac{C_{^{28}Si,sol}}{C_{Si,sol}} R_{pre} \cdot \upsilon_{pre} \cdot A_{pre} \quad (30)$$

$$\left(\frac{d^{29}Si}{dt}\right)_{Ka} = R_{Ex} - \frac{C_{^{29}Si,sol}}{C_{Si,sol}} R_{pre} \cdot \upsilon_{pre} \cdot A_{pre} \quad (31)$$

where $(d^{28}Si/dt)_{Ka}$ and $(d^{29}Si/dt)_{Ka}$ are the changes with time in the numbers of moles of ^{28}Si and ^{29}Si, respectively, that are incorporated on the surface of the kaolinite, and R_{ex} is the rate of the exchange reaction (mol s^{-1}) that represents the fractionation (Eq. (29)).

The rate of isotope exchange in each simulation was chosen to achieve a specific epsilon value, which was calculated by substituting Eqs. (30) and (31) into Eq. (28):

$$\varepsilon = 1000 \cdot \left(\frac{1}{\left(\frac{^{29}Si}{^{28}Si}\right)_{sol}} \cdot \left(\frac{R_{Ex} - \frac{C_{^{29}Si,sol}}{C_{Si,sol}} R_{pre} \cdot \upsilon_{pre} \cdot A_{pre}}{-R_{Ex} - \frac{C_{^{28}Si,sol}}{C_{Si,sol}} R_{pre} \cdot \upsilon_{pre} \cdot A_{pre}} \right) - 1 \right) \quad (32)$$

The $^{29}Si/^{28}Si$ ratio in the solution is calculated using the mass balance of the solution in the flow-through and the batch experiments (as is described below in Sections 3.3.1 and 3.3.2, respectively).

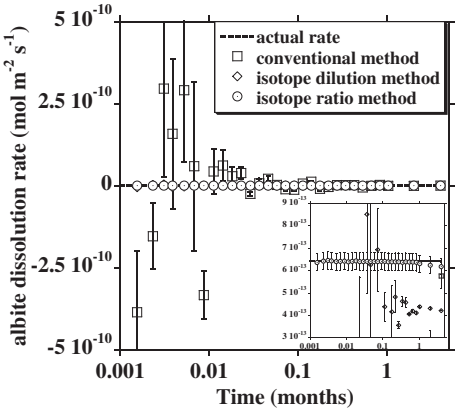

Fig. 8. The change with time in albite dissolution rates that were retrieved from the simulated concentrations and isotopic composition of a batch experiment using the conventional method, the isotope dilution method and the rates the isotope ratio method. The dashed line represents the "actual" simulated rate. The insert shows a blowup of the Y axis. The simulation conditions are described in Section 3.2.2. Error bars represent the propagated uncertainties (±2 s.d.) of the calculated rates.

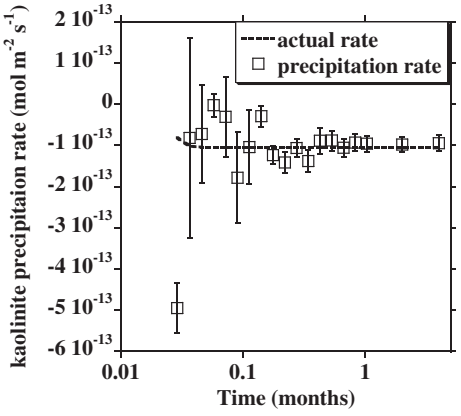

Fig. 9. The change with time in kaolinite precipitation rates that were retrieved from the simulated concentrations and isotopic composition of a batch experiment. The dashed line represents the "actual" simulated rate. The simulation conditions are described in Section 3.2.2. Error bars represent the propagated uncertainties (±2 s.d.) of the calculated rates.

The data of the change with time in Si concentrations and Si isotopic composition which was derived with the simulations with isotopic fractionation was used to derive albite dissolution rate using the isotope ratio method (Eqs. (11) and (22)), i.e., using the (wrong) assumption that there is no fractionation during kaolinite precipitation. In order to estimate the error which is solely due to isotopic fractionation, no other errors were introduced to the simulations. Thereafter, the rate of kaolinite precipitation was calculated by subtracting the release rate of Si that was calculated using the isotope dilution method from the rate that was calculated using the isotope ratio method (Eqs. (12) and (23)).

The resulting dissolution and precipitation rates were compared to the actual rates and the error due to isotope fractionation was calculated as:

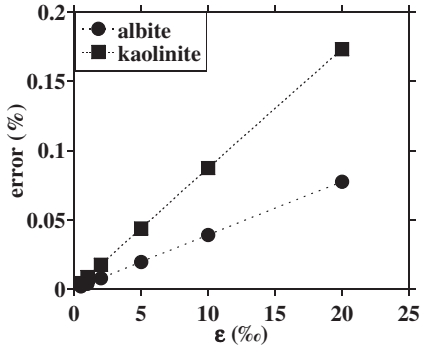

Fig. 10. The error (%) due to isotopic fractionation (ε units) in albite dissolution rates and kaolinite precipitation rates that were derived from simulated flow-through experiments using the proposed method.

$$error(\%) = \frac{Rate_{actual} - rate_{calculated}}{Rate_{actual}} \times 100 \tag{33}$$

3.3.1. Simulations of flow-through experiments with isotopic fractionation

Adding fractionation to the steady-state mass balance of ^{28}Si (Eq. (8)) and ^{29}Si in the solution gives:

$$\left(\frac{^{28}Si}{^{total}Si}\right)_{dis} \cdot R_{dis} \cdot \upsilon_{dis} \cdot A_{dis} + \left(\frac{^{28}Si}{^{total}Si}\right)_{out} R_{pre} \cdot \upsilon_{pre} \cdot A_{pre} + R_{ex} = q \cdot \left(\left(\frac{^{28}Si}{^{total}Si}\right)_{out} \cdot C_{Si,out} - \left(\frac{^{28}Si}{^{total}Si}\right)_{inf} \cdot C_{Si,inf}\right) \tag{34}$$

$$\left(\frac{^{29}Si}{^{total}Si}\right)_{dis} \cdot R_{dis} \cdot \upsilon_{dis} \cdot A_{dis} + \left(\frac{^{29}Si}{^{total}Si}\right)_{out} R_{pre} \cdot \upsilon_{pre} \cdot A_{pre} - R_{ex} = q \cdot \left(\left(\frac{^{29}Si}{^{total}Si}\right)_{out} \cdot C_{Si,out} - \left(\frac{^{29}Si}{^{total}Si}\right)_{inf} \cdot C_{Si,inf}\right) \tag{35}$$

Rearranging Eqs. (34) and (35) gives:

$$^{28}Si_{out} \cdot \left(\frac{q \cdot C_{Si,out} - R_{pre} \cdot \upsilon_{pre} \cdot A_{pre}}{^{total}Si_{out}}\right) = q \cdot \left(\frac{^{28}Si}{^{total}Si}\right)_{inf} \cdot C_{Si,inf} + \left(\frac{^{28}Si}{^{total}Si}\right)_{dis} \cdot R_{dis} \cdot \upsilon_{dis} \cdot A_{dis} + R_{ex} \tag{36}$$

$$^{29}Si_{out} \cdot \left(\frac{q \cdot C_{Si,out} - R_{pre} \cdot \upsilon_{pre} \cdot A_{pre}}{^{total}Si_{out}}\right) = q \cdot \left(\frac{^{29}Si}{^{total}Si}\right)_{inf} \cdot C_{Si,inf} + \left(\frac{^{29}Si}{^{total}Si}\right)_{dis} \cdot R_{dis} \cdot \upsilon_{dis} \cdot A_{dis} - R_{ex} \tag{37}$$

Dividing Eq. (37) by Eq. (36) gives:

$$\left(\frac{^{29}Si}{^{28}Si}\right)_{out} = \frac{q \cdot \left(\frac{^{29}Si}{^{total}Si}\right)_{inf} \cdot C_{Si,inf} + \left(\frac{^{29}Si}{^{total}Si}\right)_{dis} \cdot R_{dis} \cdot \upsilon_{dis} \cdot A_{dis} - R_{ex}}{q \cdot \left(\frac{^{28}Si}{^{total}Si}\right)_{inf} \cdot C_{Si,inf} + \left(\frac{^{28}Si}{^{total}Si}\right)_{dis} \cdot R_{dis} \cdot \upsilon_{dis} \cdot A_{dis} + R_{ex}} \tag{38}$$

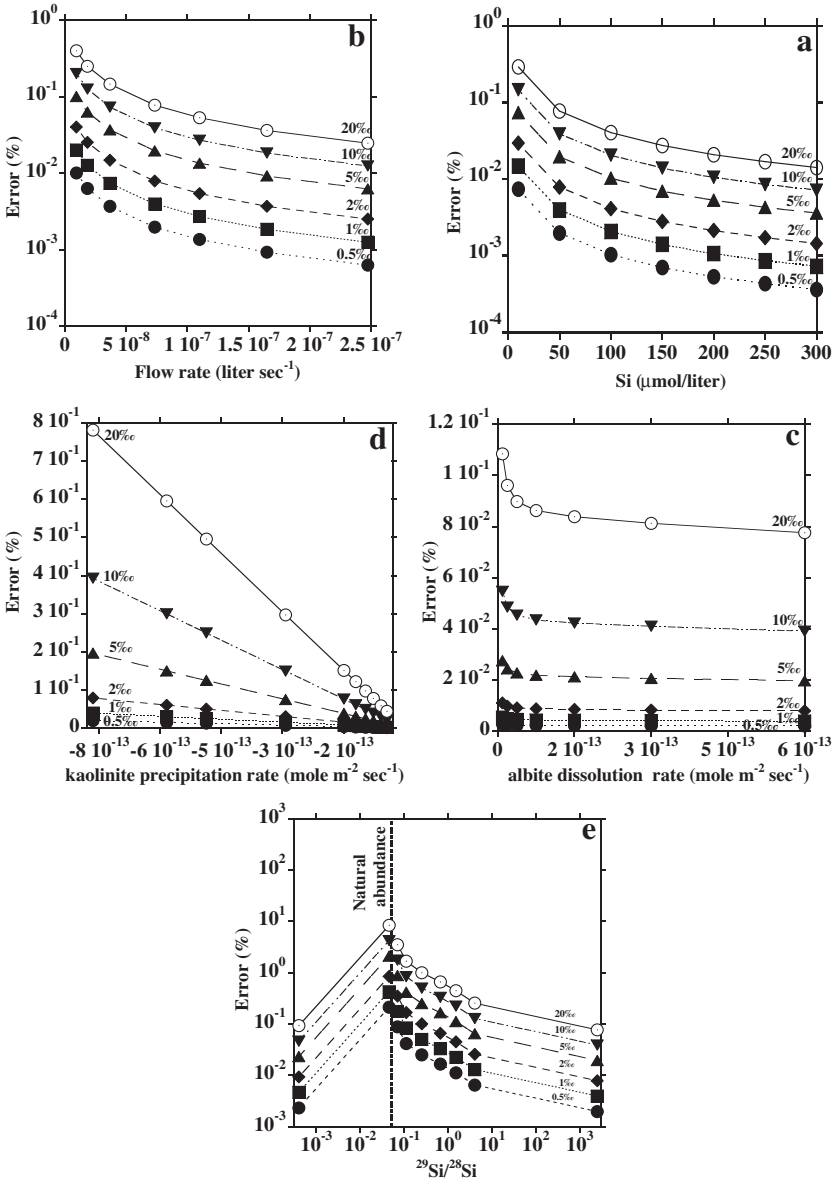

Fig. 11. The error on calculated albite dissolution rate (%) due to isotopic fractionation (ε units) as a function of (a) silicon concentration of the inflow solution; (b) flow rate; (c) albite dissolution rate; (d) kaolinite precipitation rate; and (e) the $^{29}Si/^{28}Si$ ratio in the experimental spike. The different lines and symbols represent simulation with different fractionation factor.

The basic conditions of the following flow-through simulations are identical to those in the flow-through simulation without fractionation described in Section 3.2.1, above. Si concentration and Si isotopic composition in steady state were calculated using Eqs. (7) and (38), respectively. Albite dissolution rate was calculated based on the simulated data using the isotope ratio method with the (wrong) assumption that there is no fractionation during kaolinite precipitation (Eq. (11)). Fig. 10 shows that the percentage of the error in the calculation of albite dissolution rate increased approximately linearly with the fractionation from 0.002% for fractionation of 0.5‰ to 0.08% for fractionation of 20‰. Even at the highest fractionation factors that were simulated the error was significantly less than the uncertainties in rates due to analytical uncertainties (>10%). The percentage of the error in the calculation of kaolinite precipitation rate was about double that for albite dissolution and also increased approximately linearly with the fractionation factor from 0.004% for fractionation of 0.5‰ to 0.17% for fractionation of 20‰. These errors are much smaller than the uncertainties associated with the determination of the rate of kaolinite precipitation (~7%).

As will be shown below, the errors due to the assumption that there is no fractionation depend also on different parameters of the experiments. However, changes in these parameters are not independent of each other. For example, increasing flow rate would decrease the residence time of Si and therefore its steady-state concentration, and as a result the degree of saturation with respect to kaolinite and albite would vary and consequently their reaction rate. Therefore,

changing flow-rate would affect the error due to fractionation both directly due to the change in Si residence time and indirectly by the effect of reaction rate on the error. To independently examine the direct effect of each of the parameters on the error due to fractionation, all the parameters in the model were fixed while one parameter was varied, e.g., when the inflow concentration of Si was changed the reaction rates remain constant, regardless the change in degree of saturation.

To examine the effect of silicon concentration in the inflow solution on the dissolution rate error on a given fractionation factor, the inflow solution silicon concentrations (with same isotopic composition) was varied in the range of 10–300 μM. Fig. 11a shows that for all fractionation factors, the errors decrease with increasing Si concentration. Regardless of the fractionation factor and the Si concentration the error is less than 0.7% over the range of concentrations which was examined. It is important to note that for inflow solution of 10 μM or less, the difference in concentrations between the inflow and the outflow are sufficiently large to use the conventional method.

The flow rate controls the residence time of the solutions inside the reactor in flow-through experiments, and therefore for a constant dissolution rate, increasing flow rate decreases the difference in silicon concentration between the inflow and the outflow solutions. The error due to fractionation decreases with the increase in flow rate (Fig. 11b). The magnitude of the effect is similar to that of the change in silicon concentration. Typically, flow-through experiments are not conducted with flow rates of less than 10^{-8} L s^{-1} (<1 ml/day). For such flow rates, the error due to fractionation is less than 0.4%.

The effects of albite dissolution rate and kaolinite precipitation rate on the error due to isotope fractionation are shown in Fig. 11c and d, respectively. Decreasing the dissolution rate until 4×10^{-14} mol $m^{-2}s^{-1}$ hardly affects the error. For slower dissolution rates decreasing the rate by a factor of 2 increase the error by less than 0.1% even for the highest fractionation factor. In contrast, the error due to fractionation increases linearly with increasing precipitation rate. However, even after increasing the basic rate by an order of magnitude (to -7.9×10^{-13} mol m^{-2} s^{-1}) the error is less than 1% for the highest fractionation factor ($\varepsilon = 20‰$).

In the simulation we used an experimental spike solution which was highly enriched with ^{29}Si ($^{29}Si/^{28}Si = 2497.5$, compared to the natural ratio of 0.05). The degree of enrichment increases the sensitivity of the isotope ratio method and decreases the analytical uncertainty. Fig. 11e shows that decreasing this ratio in the experimental spike also increases the error due to isotope fractionation. However, even with solution with small isotopic enrichment ($^{29}Si/^{28}Si = 0.07$, compared to the natural ratio of 0.05) the error is less than 4% for the highest fractionation factor ($\varepsilon = 20‰$).

3.3.2. Simulations of batch experiments with isotopic fractionation

Adding fractionation to the mass balance equations of ^{28}Si and ^{29}Si in the solution (Eqs. (17) and (18)) gives:

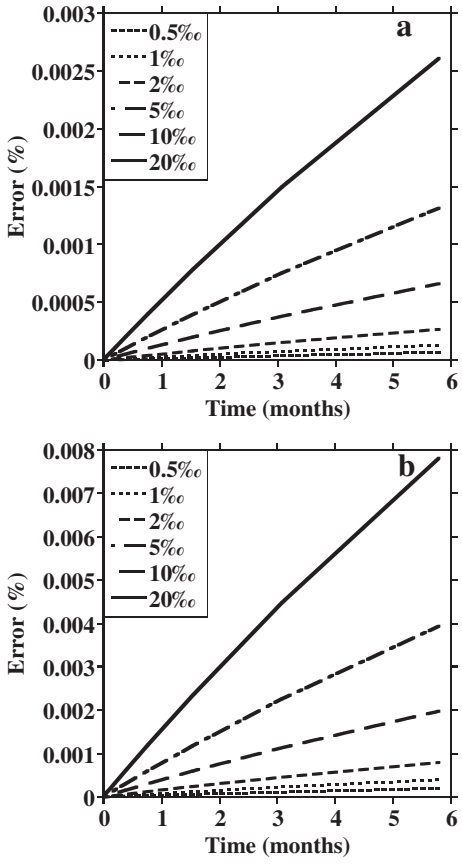

Fig. 12. The change with time of errors due to isotopic fractionation on rates that were derived from a simulated batch experiments using the proposed method: (a) calculated albite dissolution rates; and (b) calculated kaolinite precipitation rates. The different lines represent simulation with different fractionation factors.

$$\frac{d^{28}Si}{dt} = \upsilon_{Si,dis} \cdot A_{dis} \cdot R_{dis} \cdot \left(\frac{^{28}Si}{^{total}Si}\right)_{dis} + \upsilon_{Si,pre} \cdot A_{pre} \cdot R_{pre} \cdot \left(\frac{^{28}Si}{^{total}Si}\right)_{t} + R_{ex} \quad (39)$$

$$\frac{d^{29}Si}{dt} = \upsilon_{Si,dis} \cdot A_{dis} \cdot R_{dis} \cdot \left(\frac{^{29}Si}{^{total}Si}\right)_{dis} + \upsilon_{Si,pre} \cdot A_{pre} \cdot R_{pre} \cdot \left(\frac{^{29}Si}{^{total}Si}\right)_{t} - R_{ex} \quad (40)$$

Rearranging Eqs. (39) and (40) gives:

$$\upsilon_{Si,pre} \cdot A_{pre} \cdot R_{pre} \cdot \left(\frac{^{28}Si}{^{total}Si}\right)_{t} = \frac{d^{28}Si}{dt} - \upsilon_{Si,dis} \cdot A_{dis} \cdot R_{dis} \cdot \left(\frac{^{28}Si}{^{total}Si}\right)_{dis} - R_{ex} \quad (41)$$

$$\upsilon_{Si,pre} \cdot A_{pre} \cdot R_{pre} \cdot \left(\frac{^{29}Si}{^{total}Si}\right)_{t} = \frac{d^{29}Si}{dt} - \upsilon_{Si,dis} \cdot A_{dis} \cdot R_{dis} \cdot \left(\frac{^{29}Si}{^{total}Si}\right)_{dis} + R_{ex} \quad (42)$$

Dividing Eq. (42) by Eq. (41) gives:

Table 4
Analysis of samples with analytical spike. The uncertainty (2σ) in measured isotopic ratios is ±0.02% (see Section 2.5).

No.	Time (h)	$^{29}Si/^{28}Si$		$^{30}Si/^{28}Si$		Sample weight in mixture (%)	
		In	Out	In	Out	In	Out
18	3619	1.05340	1.06124	0.05493	0.05510	50.0	49.9
24	3955	1.08086	1.06352	0.05550	0.05513	50.0	50.0
30	4292	1.08736	1.06930	0.05565	0.05526	50.0	50.0
36	4627	1.13670	1.07079	0.05697	0.05529	50.0	49.9
45	5131	1.09704	1.05364	0.05587	0.05492	50.0	50.0
54	5635	1.07685	1.05205	0.05542	0.05490	50.0	50.0
60	6140	1.07719	1.04776	0.05542	0.05480	50.0	50.0
64	6380	1.07481	1.03207	0.05539	0.05444	50.0	50.0

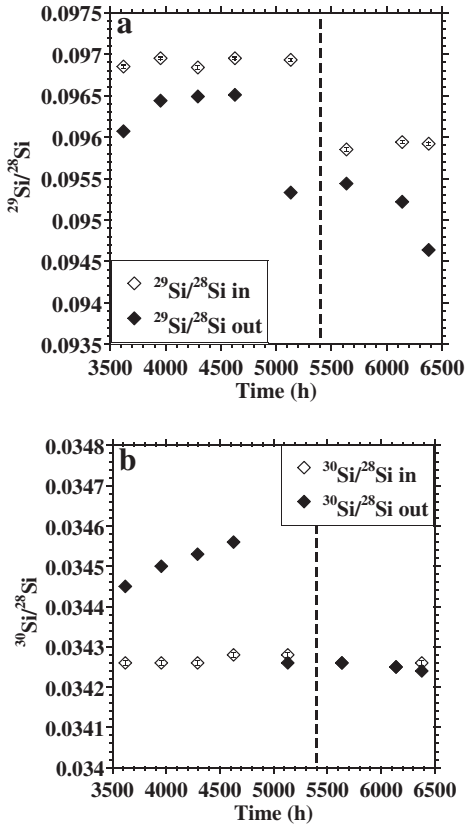

Fig. 13. The change with time in $^{29}Si/^{28}Si$ (a) and $^{30}Si/^{28}Si$ (b) ratios in the inflow and outflow solutions during a flow-through experiment. The experimental conditions are described in Table 1. Error bars represent the estimated uncertainties of the measurements (±2 s.d.).

$$\left(\frac{^{29}Si}{^{28}Si}\right)_t = \frac{\frac{d^{29}Si}{dt} - \upsilon_{Si,dis}\cdot A_{dis}\cdot R_{dis}\cdot\left(\frac{^{29}Si}{^{total}Si}\right)_{dis} + R_{ex}}{\frac{d^{28}Si}{dt} - \upsilon_{Si,dis}\cdot A_{dis}\cdot R_{dis}\cdot\left(\frac{^{28}Si}{^{total}Si}\right)_{dis} - R_{ex}} \quad (43)$$

The basic conditions of the following simulation of batch experiments are identical to those in the simulation without fractionation described in Section 3.1.2, above. The change in the concentrations of Si and of the isotopic compositions of Si with time due to albite dissolution, kaolinite precipitation and isotope fractionation was simulated using a forward model that solves Eqs. (16), (39) and (40), and the rate laws of Eqs. (24) and (25). At the end of each increment of the model the decrease in albite mass was recorded, and the albite surface area was updated using Eq. (26). Albite dissolution and kaolinite precipitation rates were calculated based on the simulated data using the isotope ratio method with the (wrong) assumption that there is no fractionation during kaolinite precipitation (Eqs. (22) and (23), respectively).

The error on calculating albite dissolution rates and kaolinite precipitation rates due to isotopic fractionation are presented in Fig. 12a and b, respectively. Although the calculated error as a result of fractionation during kaolinite precipitation increases with time, it remains negligible even for high fractionation factors (20‰). For example, the error on calculating albite dissolution rate with high fractionation factor (20‰) is less than 0.003% after almost 6 months. Moreover the error on calculating kaolinite precipitation rate, for the same fractionation factor is less than 0.01% for the same time period.

3.4. Preliminary experiment

To examine the usefulness of this new method, a preliminary flow through experiment was conducted. The experimental conditions were set such that the solutions remained far enough from equilibrium in order to be able to evaluate the rate using the conventional method (though with large uncertainty) and to compare it to the isotopic-based methods (isotope dilution and isotope ratio methods).

Aluminum and silicon concentrations and $^{29}Si/^{28}Si$, $^{30}Si/^{28}Si$ ratios at steady state are presented in Table 1. Silicon isotopic ratios of the same solutions, following the addition of the "analytical spike", are presented in Table 4.

The change with time of the isotopic composition of the samples is presented in Fig. 13. At 5400 h, a new batch of inflow solution was introduced. The $^{29}Si/^{28}Si$ ratio of the new batch (0.0959 ± 0.0001) was lower than that of the first batch (0.0969 ± 0.00005) by 0.0010 ± 0.0001. Accordingly, a similar drop of 0.0011 ± 0.0006 was observed in the average $^{29}Si/^{28}Si$ ratios of the outflow (Fig. 13a). Sample 45 (at 5131 h) shows a lower $^{29}Si/^{28}Si$ ratio values in comparison to the previous samples, which is closer to the following samples (Nos. 54, 60 and 64), even though the change in the inflow ratio occurred later in the experiment. This may indicate a contamination during the preparation of

Table 5
Calculated dissolution rate (mol m^{-2} s^{-1}).

No.	Rate by change in concentration		Rate by isotope dilution		Rate by isotope ratio	
18	7.03E-13	±248%	−2.01E-13	±739%	3.85E-13	±16%
24	8.44E-13	±214%	4.72E-13	±317%	2.66E-13	±21%
30	3.27E-14	±5644%	5.10E-13	±292%	1.85E-13	±29%
36	1.07E-12	±167%	1.72E-12	±85%	2.40E-13	±24%
45	−2.71E-13	±686%	1.18E-12	±127%	7.95E-13	±12%
54	−1.26E-12	±156%	6.66E-13	±226%	2.46E-13	±25%
60	2.42E-13	±746%	8.21E-13	±180%	3.97E-13	±17%
64	1.49E-12	±123%	1.14E-12	±131%	7.05E-13	±13%
Average	4.46E-13		7.29E-13		3.46E-13	
STDEV	9.00E-13		5.98E-13		1.76E-13	
RSD%	202%		82%		51%	
Confidence interval ($a = 0.05$)	6.67E-13		4.43E-13		1.31E-13	

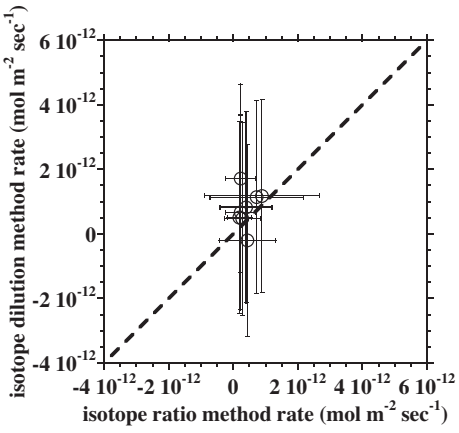

Fig. 14. Comparison of the steady-state dissolution rates in a flow through experiments that were calculated using the isotope dilution method to the rates that were calculated using the isotope ratio method. The dash line represents the agreement line (1:1). The experimental conditions are described in Table 1. Error bars represent the propagated uncertainties ±2 s.d.) of the calculated rates.

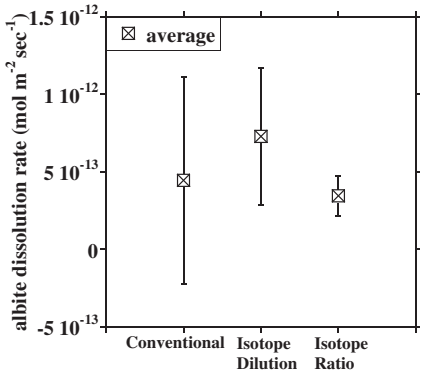

Fig. 15. Comparison of the average dissolution rates at steady state that were retrieved from the concentrations and isotopic composition of a flow-through experiments using the three different methods. Error bars represent 95% confidence interval.

this sample for analysis. Consequently, the following discussion will not take into consideration the results of sample 45. Omitting this sample does not influence the conclusion and it merely affects the noise.

Table 5 presents albite dissolution rates that were calculated using the "conventional method ", the "isotope dilution" method and the "isotope ratio" method. The rate measured by isotopic ratio is always positive (indicating dissolution), while the rate measured by other methods is negative in some samples. This is due to the small difference between the concentration of silicon in the inflow and that in the outflow solution, and a relatively large uncertainty in concentration measurements. Both the conventional method and the isotope dilution method calculate the rates from the difference between Si concentration of the outflow and the inflow solutions. As the uncertainty in determining Si using the conventional method is higher than using isotope dilution, the uncertainties of the calculated rates using the conventional method are higher than those using the isotope dilution method. Fig. 14 compares the dissolution rates calculated using the isotope dilution method to the rates that were calculated using the isotope ratio method. Since the experiment is in steady state, the rate calculated for each sample should be the same within uncertainty. As shown in Fig. 14, the scatter of the results calculated using the "isotope dilution" method (Y axis) is greater than that calculated with the "isotope ratio" method (X axis). Accordingly, the standard deviation in dissolution rate calculated with the "isotope ratio" method ($\pm 1.8 \times 10^{-13}$, Table 5) is significantly smaller than those with the isotope dilution method ($\pm 6 \times 10^{-13}$). It is important to note that the enrichment of the experimental spike solution which was used in this preliminary experiment was not high ($^{29}Si/^{28}Si \cong 0.1$, compared to the ratio of 2497.5 in the above simulations). As a result, the expected uncertainty in the experiment is higher than in the simulations. Nevertheless, the uncertainty is less than in the conventional method.

Table 5 and Fig. 15 show that there are no significant differences between the average rates calculated using the different methods, i.e., the rates are identical within 95% confidence limit. Since there is no difference in measured

rate between the methods, it is reasonable to assume that no precipitation has occurred and the negative results are due to minute difference between the concentration of silica in the inflow and outflow solution, and a relatively large uncertainty in concentration measurements (5%).

If precipitation of a secondary phase occurred during the experiment, the rate calculated with the "isotope ratio method" is supposed to be larger than the rate calculated using the other two methods mentioned in this study. Although this is not the case, it is still possible that secondary phase precipitate, but the rate of precipitation is too slow to be identified. The maximum possible precipitation rate was estimated using Eq. (12) and the average isotope ratio and isotope dilution rates, assuming that kaolinite is the secondary phase. The obtained rate equals $1.12 \pm 1.35 \times 10^{-13}$ mol s^{-1} (95% confidence limit). As the value of this average rate is positive, it is meaningless. However within uncertainty, the rate may be negative too. Therefore, within 95% confidence limit, precipitation of kaolinite may occur, but precipitation rate faster than -2.3×10^{-14} mol s^{-1} may be ruled out. The error due to possible fractionation during kaolinite precipitation was calculated as in Section 3.3.1 above, assuming that the rate of kaolinite precipitation was -2.3×10^{-14} mol s^{-1}, and found to be less than 5% even for fractionation of 20‰. Taking into account the analytical uncertainties this possible error is insignificant.

4. CONCLUSIONS AND OPEN ISSUES

Field-based dissolution rates are usually estimated by mass balance approaches in soil profiles and watersheds (see review in White and Brantley, 2003; Bricker et al., 2004) and in groundwater aquifers (e.g., Zhu, 2005). The dissolution rate of Na-rich plagioclase (albite to labradorite) in these studies ranges between 4×10^{-17} and 2×10^{-13} mol m^{-2} s^{-1} (White and Brantley, 2003). As was demonstrated by Ganor et al. (2007), it is not possible to measure field dissolution rates of silicates using standard laboratory experiments. The present study proposes and develops a new method that enables deriving slow dissolution rates of silicates close to equilibrium, with a high background Si concentration, and without the effect of secondary phase precipitation. The analytical uncertainty for the determination of dissolution rates is low for the entire range of reported field-based dissolution rates (shaded area in Fig. 6a). Moreover, the proposed method enables the estimation of the precipitation rates of the secondary phases.

The conventional methods are based on the measurements of the difference in concentrations that occur due to the dissolution. Consequently, they are: (1) limited by the analytical ability to measure these differences; and (2) changes in solution concentrations due to other processes. As a result of (1), the conventional methods enable measurements of relatively fast reactions even in the presence of silicon concentration and somewhat slower reactions when the background concentration of silicon is very low; and as a result of (2), precipitation of secondary minerals introduce error to the determined rate. Under natural conditions dissolution rates are very slow, silicon concentration is relatively high, and precipitation of secondary minerals is common, and therefore it is not possible to use the conventional methods to measure dissolution rate under close to natural conditions.

The proposed "isotope ratio method" is based on the measurements of the difference in isotopic composition that occur due to the dissolution. Consequently, they are: (1) limited by our analytical ability to measure these differences; and (2) changes in the isotopic composition of the solution due to other processes. The proposed method overcomes (1) by preforming experiments under close to natural condition but with isotopically enriched solutions that have an isotopic composition which is very different from the natural one. This and the high precision in determination of ratios of silicon isotopes using MC-ICP-MS enable measuring very slow dissolution rates with high precision.

When using the proposed "isotope ratio method" one must examine all the possible processes that may affect the silicon isotope ratio of the solution. Previous studies (e.g., Ziegler et al., 2005a; Ziegler et al., 2005b; Georg et al., 2007) showed that silicon isotopic fractionation occurs during weathering and soil development, leading to light secondary mineral phases and to isotopically heavy dissolved phases. Estimations of the fractionation factor of ^{30}Si varies but are less than 3‰, and more likely less than 2‰ (De La Rocha et al., 2000; Ziegler et al., 2005a; Ziegler et al., 2005b; Georg et al., 2006; Georg et al., 2007; Georg et al., 2009; Opfergelt et al., 2011; Opfergelt et al., 2012). As the fractionation is mass-dependent (Georg et al., 2007), the expected fractionation of ^{29}Si during the formation of clay minerals should be less than 1.5‰. In the present study, the effect of much larger isotopic fractionations (up to ε values of 20‰) was examined, and it was demonstrated that the effect of isotope fractionation during precipitation on the obtained dissolution rate was negligible both in the simulations and in the preliminary experiments. It seems that the effect of possible fractionation on the uncertainty of the obtained rate is insignificant for most of the reasonable experimental conditions. Yet, when utilizing the proposed method, one should evaluate this effect and estimate its possible outcome.

When the dissolution reaction occurred very close to equilibrium, backward precipitation of the dissolved mineral may occur even under sub-saturation conditions. The advantage of the conventional method and the isotope dilution method is that they measure only the net change in concentration, and therefore they measure the net dissolution rate of the primary mineral (in the absence of secondary mineral precipitation). The isotope ratio method will be influenced by the total dissolution rate and therefore in the presence of backward reaction the measured dissolution rate will be larger than the net dissolution rate. This limitation of the method will be dealt with in future research.

ACKNOWLEDGEMENTS

The initial idea to use isotopes to overcome the obstacles in determining dissolution rate under close-to-natural conditions was proposed by Joel Blum. C. Gruber is grateful for the support by the Yossi Levy Fellowship. CZ acknowledges NSF grants EAR-

0509755 and EAR-1225733, a research grant from the State Key Laboratory of Ore Deposits at the Institute of Geochemistry-Guiyang, Chinese Academy of Sciences and Faculty Research Support Program from Indiana University. Although the work was partly sponsored by an agency of the United States Government, the views and opinions of authors expressed herein do not necessarily state or reflect those of the United States Government or any agency thereof.

APPENDIX A. SUPPLEMENTARY DATA

Supplementary data associated with this article can be found, in the online version, at http://dx.doi.org/10.1016/j.gca.2012.11.022.

REFERENCES

Anbeek C. (1993) The effect of natural weathering on dissolution rates. *Geochim. Cosmochim. Acta* **57**, 4963–4975.

Barnes I. L., Moore L. J., Machlan L. A., Murphy T. J. and Shields W. R. (1975) Absolute isotopic abundance ratios and the atomic weight of a reference sample of silicon. *J. Res. Natl. Bur. Stand. A Phys. Chem.*, 727–735.

Barrante J. R. (1974) *Applied Mathematics for Physical Chemistry*. Prentice-Hall Inc., New Jersey.

Beig M. S. and Luttge A. (2006) Albite dissolution kinetics as a function of distance from equilibrium: implications for natural feldspar weathering. *Geochim. Cosmochim. Acta* **70**, 1402–1420.

Blum A. and Stillings L. L. (1995) Feldspar dissolution kinetics. In *Chemical Weathering Rates of Silicate Minerals* (eds. A. F. White and S. L. Brantley). Mineralogical Society of America, Washington, pp. 291–351.

Bricker O. P., Jones B. and Bowser C. J. (2004) *Mass-Balance Approach to Interpreting Weathering Reactions in Watershed Systems, Surface and Ground Water, Weathering, and Soils*. Elsevier Science, Oxford, pp. 119–132.

Brunauer S., Emmett P. H. and Teller E. (1938) Adsorption of gases in multimolecular layers. *J. Am. Chem. Soc.* **60**, 309–319.

Burch T. E., Nagy K. L. and Lasaga A. C. (1993) Free energy dependence of albite dissolution kinetics at 80 °C, pH 8.8. *Chem. Geol.* **105**, 137–162.

Cardinal D., Alleman L. Y., de Jong J., Ziegler K. and Andre L. (2003) Isotopic composition of silicon measured by multicollector plasma source mass spectrometry in dry plasma mode. *J. Anal. At. Spectrom.* **18**, 213–218.

Casey W. H., Banfield J. F., Westrich H. R. and McLaughlin L. (1993) What do dissolution experiments tell us about natural weathering? *Chem. Geol.* **105**, 1–15.

Cubillas P., Kohler S., Prieto M., Causserand C. and Oelkers E. H. (2005) How do mineral coating affect dissolution rates? An experimental study of coupled $CdCO_3$ dissolution – $CdCO_3$ precipitation. *Geochim. Cosmochim. Acta* **69**, 5459–5476.

De La Rocha C. L., Brzezinski M. A. and DeNiro M. J. (2000) A first look at the distribution of the stable isotopes of silicon in natural waters. *Geochim. Cosmochim. Acta* **64**, 2467–2477.

Douthitt C. B. (1982) The geochemistry of the stable isotopes of silicon. *Geochim. Cosmochim. Acta* **46**, 1449–1458.

Drever J. I. (2003) Surface and ground water, weathering, and soils. In *Treatise on Geochemistry* (eds. H. D. Holland and K. K. Turekian). Elsevier Science, Oxford, p. 626.

Ganor J., Huston T. J. and Walter L. M. (2005) Quartz precipitation kinetics at 180 °C in NaCl solutions – implications for the usability of the principle of detailed balancing. *Geochim. Cosmochim. Acta* **69**, 2043–2056.

Ganor J., Lu P., Zheng Z. and Zhu C. (2007) Bridging the gap between laboratory measurements and field estimations of silicate weathering using simple calculations. *Environ. Geol.* **53**, 599–610.

Ganor J., Mogollon J. L. and Lasaga A. C. (1995) The effect of pH on kaolinite dissolution rates and on activation energy. *Geochim. Cosmochim. Acta* **59**, 1037–1052.

Ganor J., Mogollon J. L. and Lasaga A. C. (1999) Kinetics of gibbsite dissolution under low ionic strength conditions. *Geochim. Cosmochim. Acta* **63**, 1635–1651.

Gautier J. M., Oelkers E. H. and Schott J. (2001) Are quartz dissolution rates proportional to B.E.T. surface areas? *Geochim. Cosmochim. Acta* **65**, 1059–1070.

Georg R. B., Reynolds B. C., Frank M. and Halliday A. N. (2006) Mechanisms controlling the silicon isotopic compositions of river waters. *Earth Planet. Sci. Lett.* **249**, 290–306.

Georg R. B., Reynolds B. C., West A. J., Burton K. W. and Halliday A. N. (2007) Silicon isotope variations accompanying basalt weathering in Iceland. *Earth Planet. Sci. Lett.* **261**, 476–490.

Georg R. B., Zhu C., Reynolds B. C. and Halliday A. N. (2009) Stable silicon isotopes of groundwater, feldspars, and clay coatings in the Navajo Sandstone aquifer, Black Mesa, Arizona, USA. *Geochim. Cosmochim. Acta* **73**, 2229–2241.

Helgeson H. C., Brown T. H., Nigrini A. and Jones T. A. (1970) Calculation of mass transfer in geochemical processes involving aqueous solutions. *Geochim. Cosmochim. Acta* **34**, 569–592.

Helgeson H. C., Murphy W. M. and Aagaard P. (1984) Thermodynamic and kinetic constraints on reaction rates among minerals and aqueous solutions. II. Rate constants, effective surface area, and the hydrolysis of feldspar. *Geochim. Cosmochim. Acta* **48**, 2405–2432.

Koroleff F. (1976) Determination of silicon. In *Methods of Seawater Analysis* (ed. K. Grasshoff). Verlag Chemie, Weinheim, pp. 149–158.

Lasaga A. C. (1998) *Kinetic Theory in the Earth Sciences*. Princeton University Press, Princeton, NJ.

Maher K., Steefel C. I., White A. F. and Stonestrom D. A. (2009) The role of reaction affinity and secondary minerals in regulating chemical weathering rates at the Santa Cruz Soil Chronosequence, California. *Geochim. Cosmochim. Acta* **73**, 2804–2831.

Metz V., Raanan H., Pieper H., Bosbach D. and Ganor J. (2005) Towards the establishment of a reliable proxy for the reactive surface area of smectite. *Geochim. Cosmochim. Acta* **69**, 2581–2591.

Nagy K. L. and Lasaga A. C. (1992) Dissolution and precipitation kinetics of gibbsite at 80 °C and pH-3 – the dependence on solution saturation state. *Geochim. Cosmochim. Acta* **56**, 3093–3111.

Nugent M. A., Brantley S. L., Pantano C. G. and Maurice P. A. (1998) The influence of natural mineral coatings on feldspar weathering. *Nature* **395**, 588–591.

Opfergelt S., Georg R. B., Burton K. W., Guicharnaud R., Siebert C., Gislason S. R. and Halliday A. N. (2011) Silicon isotopes in allophane as a proxy for mineral formation in volcanic soils. *Appl. Geochem.* **26**(Suppl.), S115–S118.

Opfergelt S., Georg R. B., Delvaux B., Cabidoche Y. M., Burton K. W. and Halliday A. N. (2012) Silicon isotopes and the tracing of desilication in volcanic soil weathering sequences, Guadeloupe. *Chem. Geol.* **326–327**, 113–122.

Parkhurst D. L. and Appello A. A. J. (1999) User's guide to PHREEQC (version 2) – a computer program for speciation, batch-reaction, one dimensional transport, and inverse geochemical modeling. Water-Resource Investigation Report 99–4259. U.S. Geological Survey, p. 312.

Schnoor J. L. (1990) Kinetics of chemical weathering: a comparison of laboratory and field weathering rates. In *Aquatic Chemical Kinetics: Reaction Rates of Processes in Natural Waters* (ed. W. Stumm). J. Wiley & Sons, pp. 475–504.

Steefel C. I. and Maher K. (2009) Fluid–rock interaction: a reactive transport approach in Thermodynamics and Kinetics of Water–Rock Interaction. In *Reviews in Mineralogy* (eds. J. Schott and E. Oelkers). Mineralogical Society of America and the Geochemical Society, pp. 495–532

Stumm W. (1992) *Chemistry of the Solid–Water Interface. Processes at the Mineral–Water and Particle–Water Interface in Natural Systems*. John Wiley & Sons, Inc., New York.

van Grinsven H. J. M. and van Riemsdijk W. H. (1992) Evaluation of batch and column techniques to measure weathering rates in soils. *Geoderma* **52**, 41–57.

Velbel M. A. (1993) Constancy of silicate-mineral weathering-rate ratios between natural and experimental weathering: implications for hydrologic control of differences in absolute rates. *Chem. Geol.* **105**, 89–99.

White A. F. and Brantley S. L. (1995) Chemical weathering rates of silicate minerals. In *Reviews in Mineralogy* (ed. P. H. Ribbe). Mineralogical Society of America, Washington, p. 583.

White A. F. and Brantley S. L. (2003) The effect of time on the weathering of silicate minerals: why do weathering rates differ in the laboratory and field? *Chem. Geol.* **202**, 479–506.

Wieland E. and Stumm W. (1992) Dissolution kinetics of kaolinite in acidic aqueous solutions at 25 °C. *Geochim. Cosmochim. Acta* **56**, 3339–3355.

Zhu C. (2005) In situ feldspar dissolution rates in an aquifer. *Geochim. Cosmochim. Acta* **69**, 1435–1453.

Zhu C., Blum A. and Veblen D. (2004) Feldspar dissolution rates and clay precipitation in the Navajo aquifer at Black Mesa, Arizona, USA. In *11th International Symposium on Water–Rock Interaction WRI-11* (eds. R. B. Wanty and R. R. Seal). Balkema, Saratoga Springs, NY, USA, pp. 895–899.

Zhu C., Lu P., Zheng Z. and Ganor J. (2010) Coupled alkali feldspar dissolution and secondary mineral precipitation in batch systems: 4. Numerical modeling of kinetic reaction paths. *Geochim. Cosmochim. Acta* **74**, 3963–3983.

Ziegler K., Chadwick O. A., Brzezinski M. A. and Kelly E. F. (2005a) Natural variations of δ^{30}Si ratios during progressive basalt weathering, Hawaiian Islands. *Geochim. Cosmochim. Acta* **69**, 4597–4610.

Ziegler K., Chadwick O. A., White A. F. and Brzezinski M. A. (2005b) Δ^{30}Si systematics in a granitic saprolite, Puerto Rico. *Geology* **33**, 817–820.

Associate editor: Andrew Jacobson